Imaging of COPD

8

Sang Min Lee, Song Soo Kim, Hye Jeon Hwang, and Joon Beom Seo

Computed Tomography (CT)

CT Basic Physics

Computed tomography (CT) of the thorax is a very quick and the most advanced imaging technique. CT scanner is designed to use a form of gantry which allows rotation of the X-ray tube and the detector around the patient during breath hold. With the development of CT technology, single breath-hold scanning of the thorax can be achieved, and image reconstruction of sagittal and coronal planes is also feasible with minimal loss of spatial resolution. During the decades, the fan beam of a CT scanner is broadened along the *Z*-axis and two-dimensional detectors are developed, acquisition of a number of slices per rotation is possible. Recently developed multi-slice and multi-detector CT allows cone beam CT and volumetric imaging. After CT scan, the X-ray attenuation, called tissue density, is expressed as a Hounsfield Units (HU). The scale of HU values range from −1000 HU (attenuation value of air) to 3000 HU, and 0 HU corresponds to the attenuation of water (Fig. 8.1). Generally, normal lung has an attenuation value around −850 HU on inspiratory CT because normal lung attenuation reflects the mixed attenuation of intrapulmonary air and lung parenchyma.

The original version of this chapter was revised. An erratum to this chapter can be found at https://doi.org/10.1007/978-3-662-47178-4_24

S.M. Lee, M.D. • J.B. Seo, M.D., Ph.D. (✉)
Division of Cardiothoracic Radiology, Department of Radiology, Asan Medical Center, University of Ulsan College of Medicine, Seoul, South Korea
e-mail: sangmin.lee.md@gmail.com; asellion@hanmail.net, joonbeom.seo@gmail.com

S.S. Kim, M.D.
Department of Radiology, Chungnam National University Hospital, Chungnam National University School of Medicine, Daejeon, South Korea
e-mail: haneul88@hanmail.net

H.J. Hwang, M.D.
Department of Radiology, Hallym University College of Medicine, Hallym University Sacred Heart Hospital, Seoul, South Korea
e-mail: umttette@hanmail.net

Radiation Dose of COPD CT

The radiation dose during CT scan is presented as the gray or mGy unit, which is proportional to the amount of energy that the irradiated body part is expected to absorb. The Sievert (Sv) unit is used in the report of the effective dose. Regarding chest CT scan for evaluation of chronic obstructive pulmonary disease (COPD), acceptable low dose screening and standard dose of CTs can be performed at effective dose of approximately 2 and 7 mSv, respectively [1].

CT Protocol

Optimization of CT protocol and quality control of image acquisition are critical for assessment of COPD [2, 3]. Ideally, single CT protocol using dedicated single CT scanner and software system based on exactly the same parameters of image

S.-D. Lee (ed.), *COPD*, DOI 10.1007/978-3-662-47178-4_8

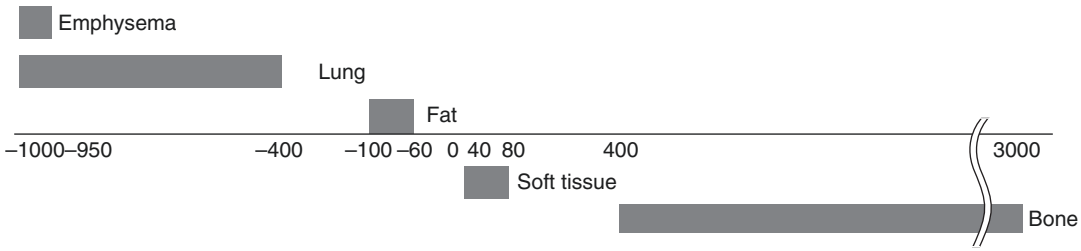

Fig. 8.1 Hounsfield unit on CT images. The Hounsfield unit (HU) is a quantitative value for describing attenuation on CT images. Zero HU and −1000 HU are defined as attenuation of distilled water and air at standard pressure and temperature. CT images can be appropriately displayed according to target organs adjusting window width and level. Window width describes the range of HU on CT image and window level is the median HU of window width. In the thorax, lung, mediastinum, and bone window setting are usually used

acquisition and reconstruction should be used. Nevertheless, it is impossible in most cases, particularly for multicenter trials. There are several important issues to be considered for the optimization of CT protocol which include kilovoltage setting, tube currents, respiration level, image thickness, reconstruction kernel, and so on (Table 8.1). Generally speaking, the volumetric CT acquisition obtained at maximal inspiration with standardized breathing instruction is essential for accurate COPD assessment using CT. Thin-section CT reconstructions (even or less than 1 mm in thickness) are required for proper characterization and quantification of emphysema and airway change in COPD. It has been known that CT estimates of emphysema severity increase as section thickness decreases and that higher frequency (edge-enhancing, sharper) image reconstruction kernel results in higher CT measurements of emphysema than lower frequency resolution (smoothing) kernel [4–6]. Low radiation dose CT scan allows the visual evaluation of emphysema, however, which trade off relatively high image noise, resulting in overestimation of emphysema extent. Relatively higher dose CT is also necessary for the accurate measurement of airway dimensions. Recently, further reduction of CT dose can be possible with the use of novel technique of iterative reconstruction [7–9]. However, it is not recommended for the quantitative assessment of COPD CT because the influence of changing reconstruction method has not been fully studied. Dose modulation technique to reduce radiation dose is not recommended. Expiratory CT is gradually regarded as an important part of COPD evaluation for the presence and distribution of air trapping on visual and quantitative assessment [10]. Expiratory CT scan may be obtained at relatively low dose after inspiratory CT acquisition. However, different noise level between inspiratory and expiratory CT is potential problem for the quantitative analysis. Expiratory scan can be obtained at the end of a tidal expiration, which corresponds to functional residual capacity, or after full expiration, which is in residual volume status.

Diagnosis of Morphologic Change in COPD

Emphysema: Definition of CT Finding, Subtype, Pathologic Correlation

Pulmonary emphysema is defined as an abnormal permanent enlargement of the airspaces distal to the terminal bronchioles, which results in lower CT attenuation values than those of normal healthy lung areas. Although pulmonary function test (PFT) is useful for clinical severity assessment of COPD, it does not represent the type and range of heterogeneous pathophysiologic abnormalities in COPD [11, 12]. In addition, it tends to be relatively insensitive to both early stages and small changes in COPD [13]. CT scan may be ideal for the detection and characterization of COPD in that it allows for an in vivo analysis of morphologic characteristics and distribution of emphysema. Visual assessment is also useful to

Table 8.1 General principle of CT protocol for COPD evaluation

	Inspiratory CT	Expiratory CT (optional)
Scan type, mode	Spiral (volumetric)	Spiral (volumetric)
Rotation time (s)	As short as possible, usually no greater than 0.5 s	As short as possible, usually no greater than 0.5 s
Detector configuration	More than 16 channels × submillimeter collimation	More than 16 channels × submillimeter collimation
Pitch	Usually smaller than 1.0	Usually smaller than 1.0
kVp	120	120
mA	40 mAs (low dose) up to 200 mAs (moderate dose)	40 mAs (low dose) up to 200 mAs (moderate dose)
Dose modulation	Not recommended	Not recommended
Reconstruction I for visual assessment		
Algorithm	Sharp or high-frequency kernel	Sharp or high-frequency kernel
Thickness (mm)	Submillimeter (0.5–0.75 mm)	Submillimeter (0.5–0.75 mm)
Interval (mm)	0.5	0.5
DFOV (cm)	To cover the whole lung	To cover the whole lung
Reconstruction II for QCT		
Algorithm	Neutral, smooth kernel	Neutral, smooth kernel
Thickness (mm)	Submillimeter (0.5–0.75 mm)	Submillimeter (0.5–0.75 mm)
Interval (mm)	0.5	0.5
DFOV (cm)	To cover the whole lung	To cover the whole lung

subtype the emphysema into centrilobular, panlobular, and paraseptal types. Centrilobular emphysema is the most common morphologic subtype of pulmonary emphysema. Pathologically, it begins near the center of the secondary pulmonary lobule (the most fundamental structural component of the lung containing parenchyma, airways, lymphatics, and vasculature) in the region of the proximal respiratory bronchiole. Parenchymal destruction starts in the center of secondary pulmonary lobule results in the characteristic apposition of normal and emphysematous lung (area of low attenuated destruction surrounded by normal tissue). On CT, small round low attenuated holes are evenly distributed with ill-defined borders in early stage and these low attenuated areas become confluent and inseparable with paucity of pulmonary vascularity in late stage (Fig. 8.2). Panlobular emphysema is characterized by permanent destruction of the entire acinus distal to the respiratory bronchiole, and its pathogenesis relates to alpha-1 antitrypsin deficiency. Parenchymal destruction involving entire acinus, which is contrast to centrilobular subtype, affects the lower lobes more severely (Fig. 8.2). Paraseptal emphysema tends to be limited in extent and occurs most commonly along the subpleural portion of the upper lung, often coexisting with other types of emphysema and fibrosis. Small focal lucencies, up to 10 mm in size, can be seen on CT (Fig. 8.2). Bullae or blebs, termed interchangeably, are focal regions of emphysema with no discernible wall, usually more than 1 cm in diameter at subpleural location. In some cases, they can be very large and may result in pneumothorax in COPD patients (Fig. 8.3).

Airway Change: Bronchus, Trachea

Bronchial wall thickening, bronchial luminal irregularity, and bronchiectasis are commonly seen in patients with COPD with mixed findings of emphysema. Bronchial wall thickening is regarded as a sign of chronic bronchitis, easily identified in heavy cigarette smokers. Pathophysiologically, irreversible and progressive histologic changes in airways show diffuse hyperplasia of mucous glands associated with hypersecretion and bronchial wall thickening. Traditionally, bronchial wall is regarded to be

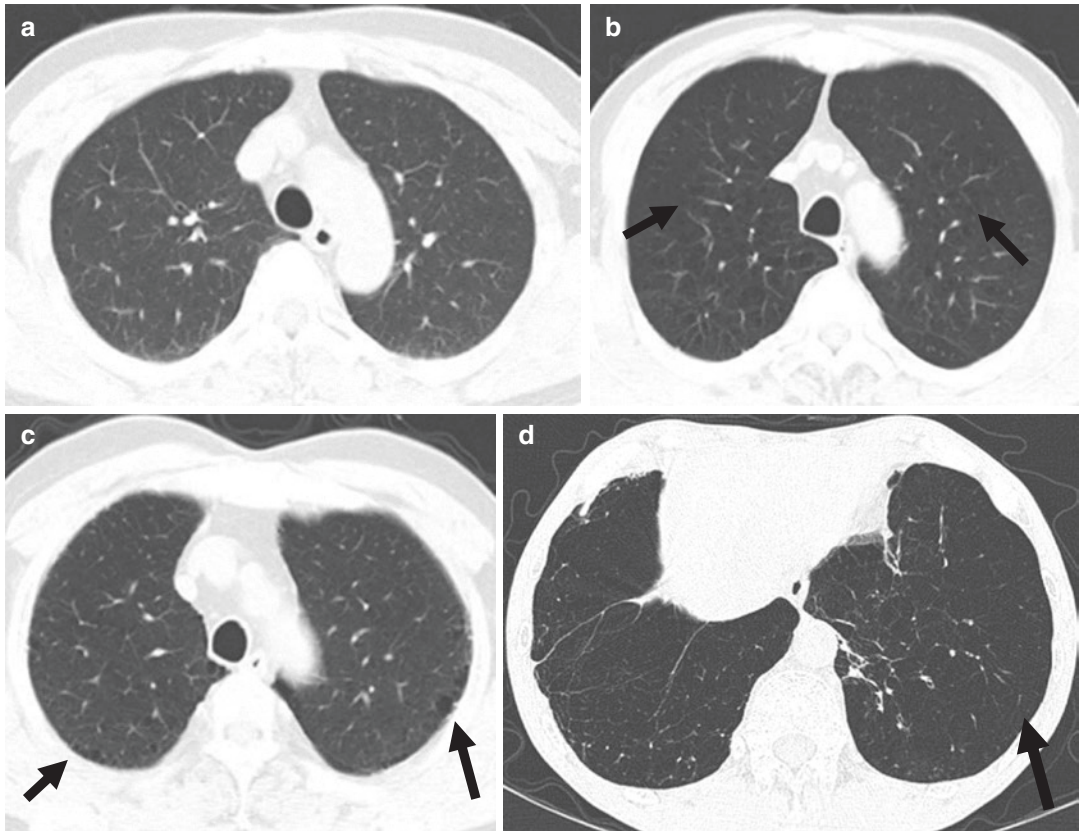

Fig. 8.2 Emphysema subtypes on CT images. (**a**) Normal lung parenchyma. (**b**) Centrilobular emphysema. Scattered small focal lucencies (parenchymal destruction) in upper lobes, measuring more or less than 1 cm in diameter. (**c**) Paraseptal emphysema. Small focal lucencies, up to 1 cm in diameter, are located in subpleural ar8ea adjacent to the pleura and septal lines. (**d**) Panlobular emphysema. Secondary pulmonary lobules area completely replaced with emphysema with showing uniform and relatively homogeneous lucencies across parts of the secondary pulmonary lobules

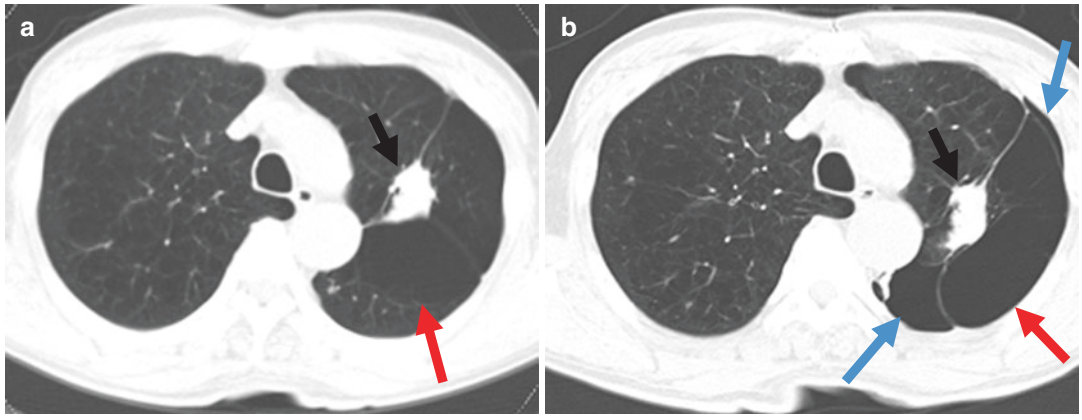

Fig. 8.3 Large bullae and pneumothorax in a COPD patients. A 71-year-old male with COPD complaint of sudden dyspnea. (**a**) CT image at 3 month ago showed large subpleural bullae with collapsed central lung. (**b**) Left pneumothorax was noted with collapsed lung and large bullae

thick if the diameter ratio of inner to outer lumen of bronchus is greater than 0.8. Nevertheless, the diagnosis of bronchial wall thickening of COPD with naked eyes on CT is subjective and still limited (Fig. 8.4). Moreover, it is virtually impossible to differentiate bronchial wall thickening of COPD from acute bronchitis or asthma. Bronchiectasis can be accompanied in COPD patients and may represent severe airflow obstruction [14, 15]. Trachea and main bronchus abnormalities can be visually defined on CT in COPD patients. Tracheobronchomalacia, saber-sheath deformity of trachea, and outpouching of trachea and main bronchus can be seen in advanced COPD (Fig. 8.5). Tracheobronchomalacia is traditionally defined as a more than 50% collapse of the trachea and main bronchus at end-expiratory CT. Saber-sheath deformity is seen as coronal narrowing and sagittal widening of the intrathoracic tracheal diameter. Tracheal outpouching is defined as a focal herniation of mucosa through the tracheal wall.

Air Trapping

It has been understood that small airway airflow resistance is the major site of obstruction in patients with COPD and precede the onset of emphysematous destruction in both centrilobular and paraseptal emphysema phenotypes of COPD [16]. Therefore, early detection and diagnosis of small airway disease in COPD is fundamental for early diagnosis of COPD. The small airways are referred to as airway lumen less than 2 mm, which cannot be visualized directly using even recently developed CT scanners. Thus, the finding of air or gas trapping, which appears to decrease lung attenuation on expiratory CT, can be used as indirect sign of small airway dysfunction in COPD because this finding is thought to be caused by early collapse of small airway on expiration. Expiratory CT is increasingly regarded as an essential tool for the evaluation of air trapping as an obstructive pattern of small airway disease in COPD patients. In many cases, especially in emphysema dominant COPD patients, the detection of small airway dysfunction may be hampered by the presence of emphysema because the lung density of emphysema area on expiration CT can be low without small airway dysfunction. In such situation, side-by-side comparison of inspiratory and expiratory CT images is necessary to detect lack of normal increase of lung attenuation and decrease of lung volume on expiration (Fig. 8.6).

Others: Chest Wall, Diaphragm, Heart, Pulmonary Vessel, and Bone

Morphologic changes secondary to pulmonary hyperinflation in COPD include chest wall

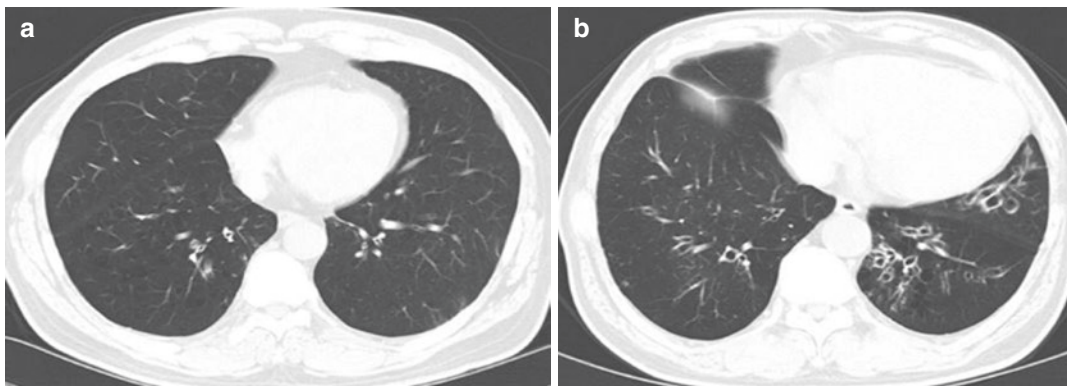

Fig. 8.4 Airway changes in COPD. (**a**) Example of bronchial wall thickening. Typical and severe thickening of wall of entire segmental bronchi in both lower lobes is noted. The diameter ratio of inner to outer lumen is smaller than 0.8. (**b**) Example of bronchiectasis. Marked dilatation of bronchial lumen in both lower lungs is noted. The inner luminal diameter of bronchus is greater than the diameter of the accompanying pulmonary artery. There are also loss of normal tapering with bronchial wall thickening

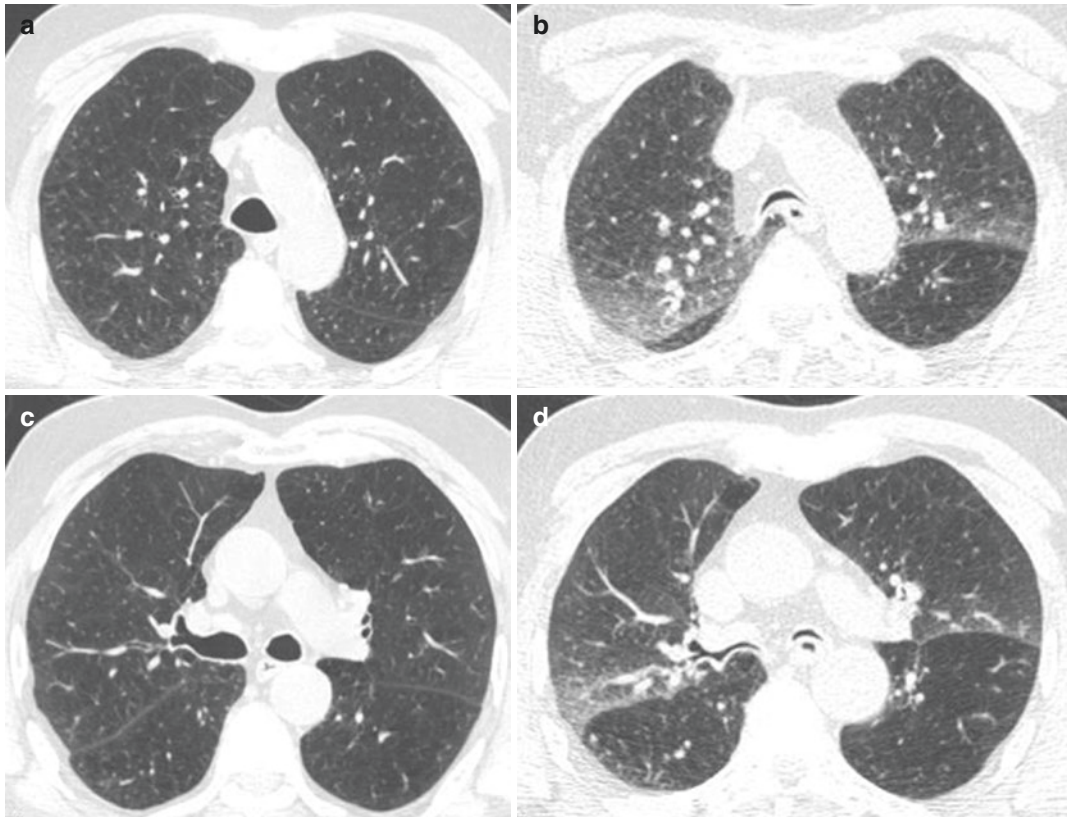

Fig. 8.5 Tracheobronchomalacia. Tracheobronchomalacia is defined as abnormal collapse of airway lumen on expiration. This abnormal finding can be seen in COPD patients. CT images on inspiration (**a**) and expiration (**b**) demonstrate severe lumen narrowing of the trachea on expiration (**b**) and CT images on inspiration (**c**) and expiration (**d**) also depicted severe lumen narrowing of both bronchi (**d**). In addition, severe air trapping is seen in both lower lobes

deformity, diaphragmatic change, changes in the heart, and pulmonary vasculatures. Barrel chest deformity is the well-known chest wall deformity of COPD and depression of diaphragm indicates the flattening of the domes of the diaphragm due to hyperinflation of the lung in COPD (Fig. 8.7). As the progression of COPD, the heart tends to be more vertically oriented due to hyperinflation of the lung. In later stage, right ventricular and atrial dilatation, dilatation of central pulmonary arteries, and acute tapering of distal pulmonary vessels can be seen as a finding of pulmonary hypertension. Osteoporosis is also one of the systemic effects associated with COPD attributed by inactivity, COPD-related systemic inflammation, the use of systemic corticosteroids, and vitamin D deficiency. Bone fracture related to osteoporosis, in turn, may also reduce pulmonary function or even cause COPD exacerbations [17].

Severity Assessment of COPD

Extent of Emphysema: Visual Assessment

Visual assessment of COPD is relatively simple, cheap, and independent from variation of CT machine or reconstruction algorithms. Furthermore, comprehensive visual emphysema assessment of CT in COPD allows assessment of the pattern, subtype, regional location, and degree of emphysema. It also has an advantage for detecting lots of accompanying pathologic changes in the parenchyma as well as in the small

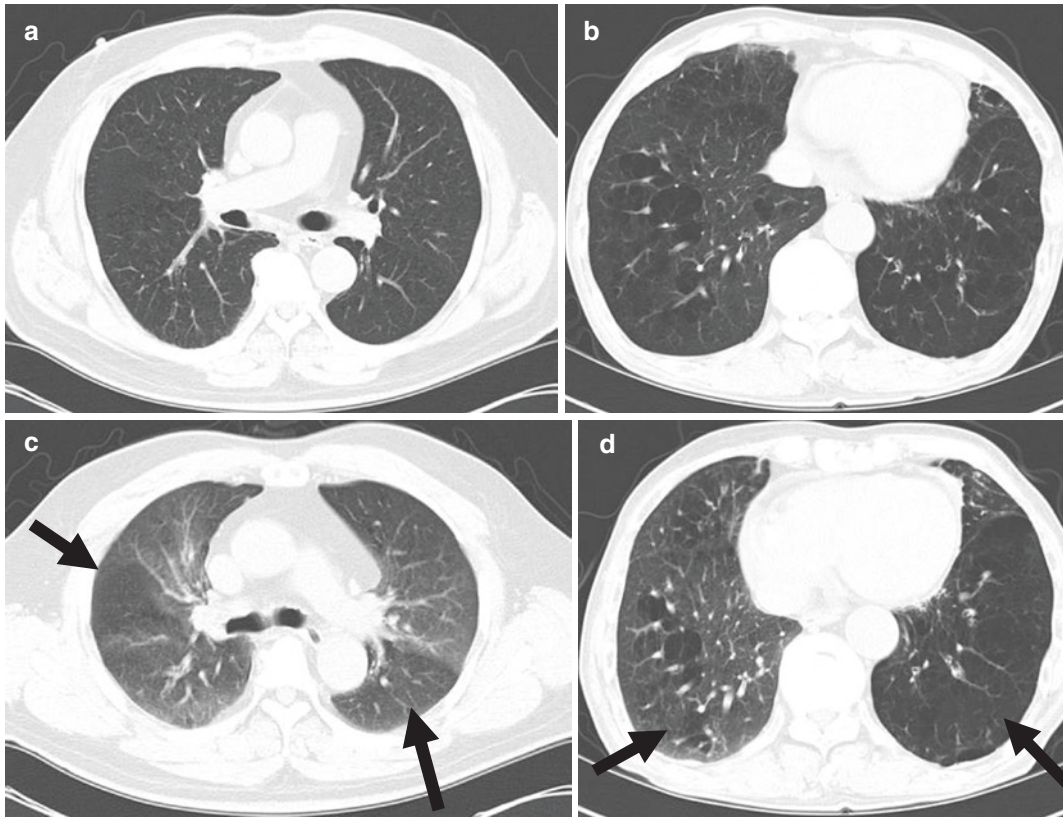

Fig. 8.6 Air trapping assessment using inspiration- and expiration CT images. Air trapping should be assessed by side-by-side comparison of inspiration (**a**, **b**) and expiration (**c**, **d**) CT images. Expiratory air trapping can be defined as areas showing lack of normal increase of lung attenuation and decrease of lung volume on expiration image (**c**, **d**). The areas of air trapping are marked in *arrows*

and large airways. Visual assessment allows for the detection of early emphysema in asymptomatic smokers even before the development of airflow limitation, which is essential for the diagnosis of COPD. It is also useful to follow the progression of emphysema over time. For the optimal evaluation of emphysema with CT images in COPD patients, thin-section, high-resolution CT images should be used at recommended window settings (usually with a window level of −700 and window width of 1000–1500). On visual assessment, emphysema is classified as centrilobular, panlobular, and paraspetal emphysema (Fig. 8.2). The extent of emphysema has been assessed by using visual scoring system [18]. Typically, the extent of emphysema in each lobe can be assessed by using a six-point scale system: 0, 1–5%, 6–25%, 26–50%, 51–75%, and greater than 75% [19]. However, main limitation of visual assessment has been the relatively low inter-reader agreement [20, 21]. The inter-reader agreement was moderate for the presence or absence of emphysema and for the presence of panlobular emphysema; fair for the presence of centrilobular and paraseptal subtypes [22]. In an effort to improve the inter-reader agreement, usage of standardized reference images has been attempted with promising results [19].

Extent of Emphysema: Computer-Based Quantification

For the objective and reproducible assessment of emphysema, computer-based quantification method, the so-called quantitative CT (QCT), has

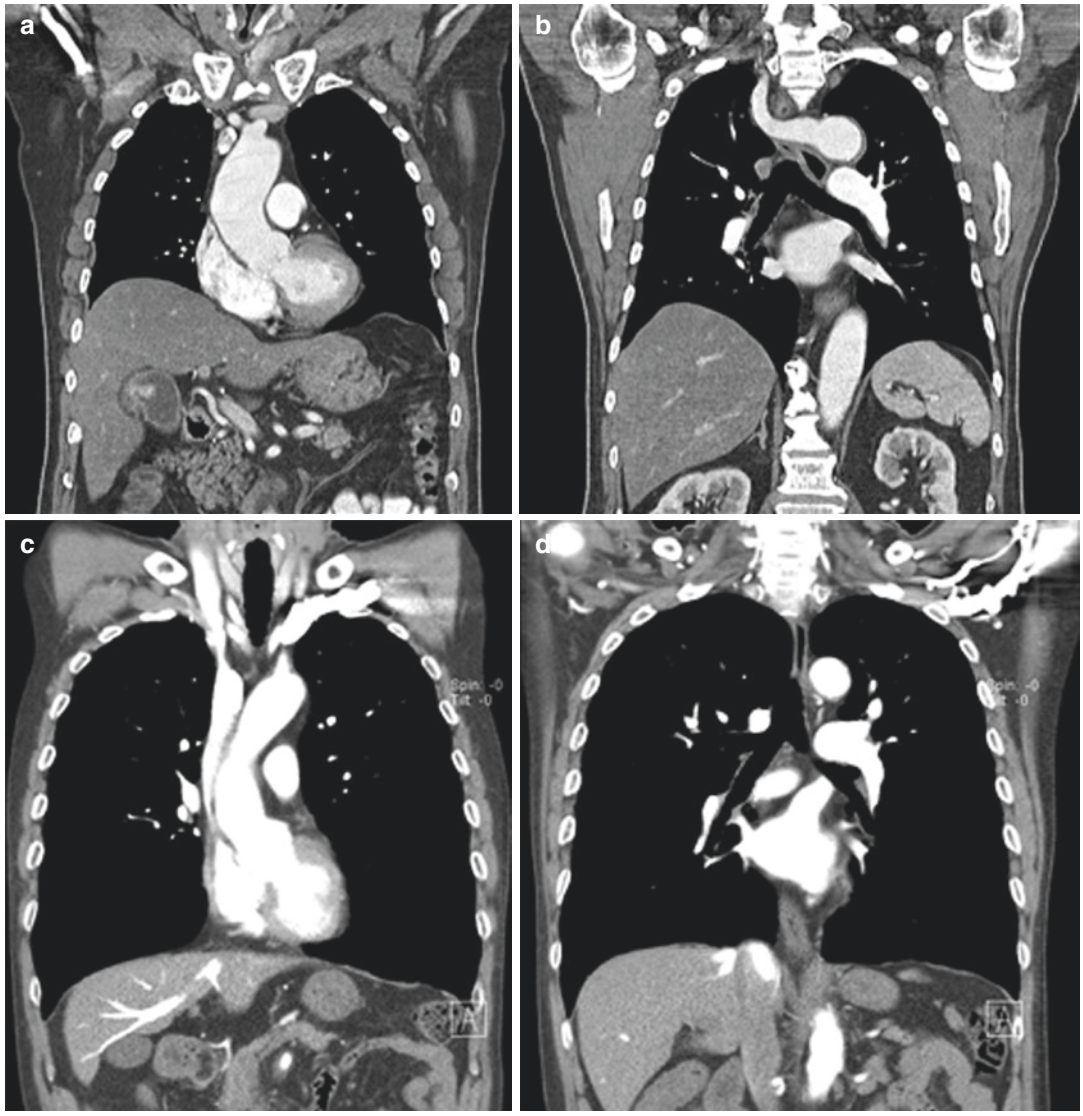

Fig. 8.7 Morphologic change of the diaphragm in COPD patients. Compared with CT images in a normal individual (**a**, **b**), coronal CT images (**c**, **d**) in a 74-year-old male with COPD shows depressed and flattened shape of the diaphragm. This change is due to hyperinflation of the lung in COPD

been introduced. As briefly explained in "CT Basic Physics" section, emphysema area on CT with relatively increased air fraction in inspiration lung is shown as area of decreased CT attenuation approaching air attenuation of −1000 HU, compared with normal lung CT attenuation around −850 HU [23]. Accordingly, if a certain threshold value is applied, the area of emphysema with decreased CT attenuation can be objectively divided from normal lung area. This method is called as "density mask" and the threshold of −910 HU was initially applied [24]. Recent studies using thin-section, multi-detector CT scanners showed that the highest correlation between QCT and histology is found when the threshold set at −960 or −970 HU [25]. However, the lower the thresholds, the more sensitive the image noise; therefore, the threshold of −950 HU is now most commonly used. When the correction for lung volume changes influenced by

degree of inspiration is applied, this quantitative method for emphysema is near perfectly reproducible method. The term of percent of emphysema (emphysema index, EI or $\%LAA_{-950}$) stands for the relative area of lung less than −950 HU (Figs. 8.8 and 8.9). Another method is using the nth cutoff percentile in the attenuation distribution curve using the CT attenuation at a certain percentile along the frequency histogram of pulmonary parenchymal attenuation (density value in HU under which n% of frequency histogram) (Fig. 8.8). This value is called as "percentile index," and it is reported that it has an advantage on longitudinal evaluation and less sensitive to lung volume changes [26–28]. The first percentile value is much optimal for correlation with histology; however, it is known to be sensitive to an artifact from image noise and truncation effect. Instead, the 15th percentile threshold is commonly used [28, 29]. The last method is to assess the mean of the whole lung attenuation (mean lung density, MLD). Regional heterogeneity of emphysema can be assessed quantitatively to assess the regional distribution of emphysema. Most available QCT methods can divide each lung into upper, mid, and lower zones of equal height or volume, and ratios between the extent of emphysema in upper and lower lung can be computed. Newer methods can also permit segmentation of lobes to compute lobar volumes and extent of emphysema objectively (Fig. 8.9).

Comparison Between Visual Assessment and CT Quantification

In the assessment of emphysema in COPD patients, although QCT measures correlate with the severity of visual CT assessment, the level of correlation is only moderate [22]. Especially in less severe categories of emphysema, visual assessment by radiologists tends to be usually underestimated for the extent of emphysema when compared to QCT measures, while in those with more severe emphysema, the radiologists tend to relatively overestimate the emphysema extent [30]. Therefore, visual assessment and QCT measures should be used complementarily and performed independently for the assessments of severity of emphysema.

Correlation Between the Extent of Emphysema and Clinical Parameters

Visual, subjective assessment of the emphysema using contiguous 10-mm thick CT started in 1986, there were significant correlations between CT visual scores and macroscopic emphysema. However, even with the development of high-resolution CT, visual grading assessment is not really a quantitative measure but just grading the degree of emphysema according to categories of emphysema severity. Recently, using pulmonary lobe-by-lobe visual assessment, severity of emphysema correlates quite well with physiologic parameters (FEV_1 and FEV_1/FVC) and GOLD stage [19]. The correlation coefficient ranges between 0.67 (for GOLD stage) and −0.74 (for FEV_1/FVC) and notably the range of correlation coefficients are similar to the correlations between extent of emphysema on QCT and each physiologic parameter (0.62 for GOLD stage and −0.70 for FEV_1/FVC). However, inter-reader agreement regarding severity of emphysema on visual assessment tends to be variable, so QCT is preferred for assessing disease severity of emphysema. Moreover, QCT measurements have shown to correlate better than visual CT assessment with macroscopic measurement of emphysema [21].

Regional Heterogeneity of Emphysema

Severity and distribution of emphysema differs in lung regions such as core (inner) vs. rind (outer), upper vs. lower, even among each lobe (Fig. 8.10). There have been several reports regarding regional variation of emphysema. Basal distribution of emphysema is associated with greater impairment of FEV_1 but less impairment of gas exchange (PaO_2) and alveolar-arterial oxygen gradient than the apical distribution of emphysema [31]. Emphysema areas on CT are more often found in the inner segment of the lung than in the outer segment and the extent of emphysema in inner segment of the lower lung in QCT is much more clearly correlated with airflow limitation than those in outer segment [32]. In another report applying the slope of the EI in the upper-lower, anterior-posterior, and central-peripheral direction in both side lung, the heterogeneity of emphysema distribution in

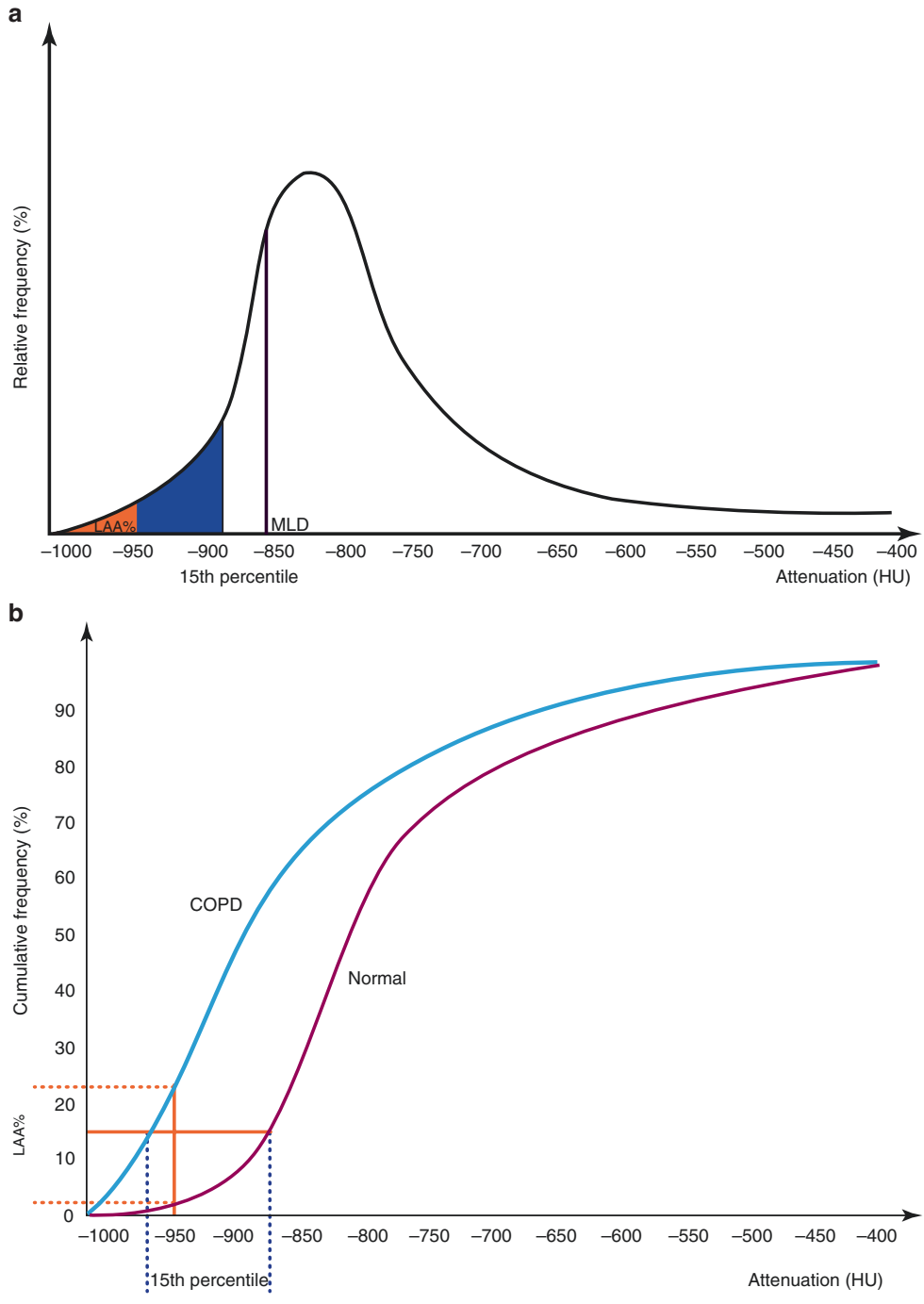

Fig. 8.8 Quantitative CT measurements of emphysema regarding LLA%, percentile index, and mean lung density (MLD). The concept of QCT measurement is illustrated in Fig. (**a**). Frequency distribution curves are plotted according to the apparent X-ray attenuation values. The threshold of −400 HU is to define lung area. Threshold (LAA %) technique uses a predefined threshold of HU (i.e., –950 HU) is chosen and the percentage of lung less than this value can be calculated. Contrary to this, the percentile index method uses a certain percentile point (i.e., lowest 15th percentile) and the HU value for that percentile is calculated. The last index is the mean of lung density (MLD). Left side shift of frequency curve in patient with emphysema is demonstrated in Fig. (**b**). As a result of the shift, LAA % increases and percentile index decreases in patients with emphysema. The area of emphysema can be overlaid on the CT images to highlight the emphysema lesion (**c**, **d**)

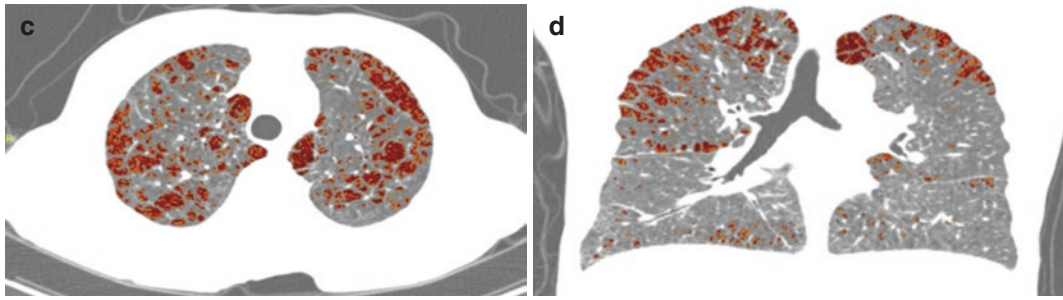

Fig. 8.8 (continued)

Fig. 8.9 Lobar-specific quantification of emphysema. Example of software providing automatic segmentation of lobes and quantitative assessment of extent of emphysema at the whole lung and lobar level

anterior-posterior and upper-lower direction was independent determinants of FEV_1 and FEV_1/FVC and the lower and posterior regional dominant emphysema is associated with a decrease in FEV_1 and FEV_1/FVC [33]. Regional assessment using QCT helps in selecting candidates for lung volume reduction surgery (LVRS) and provides rationale for the mechanisms of improvement after LVRS (Fig. 8.11). The extent of emphysema of the upper-rind region of the lungs is a significant predictor for improvement of pulmonary function after LVRS [34].

Airway Change: Visual Assessment

Although visual assessment of large airways is a subjective process, the presence of airway wall thickening or dilation of large airways can represent bronchial inflammation with remodeling, and it also contributes to the symptomatic exacerbation in COPD patients. Bronchial wall thickening

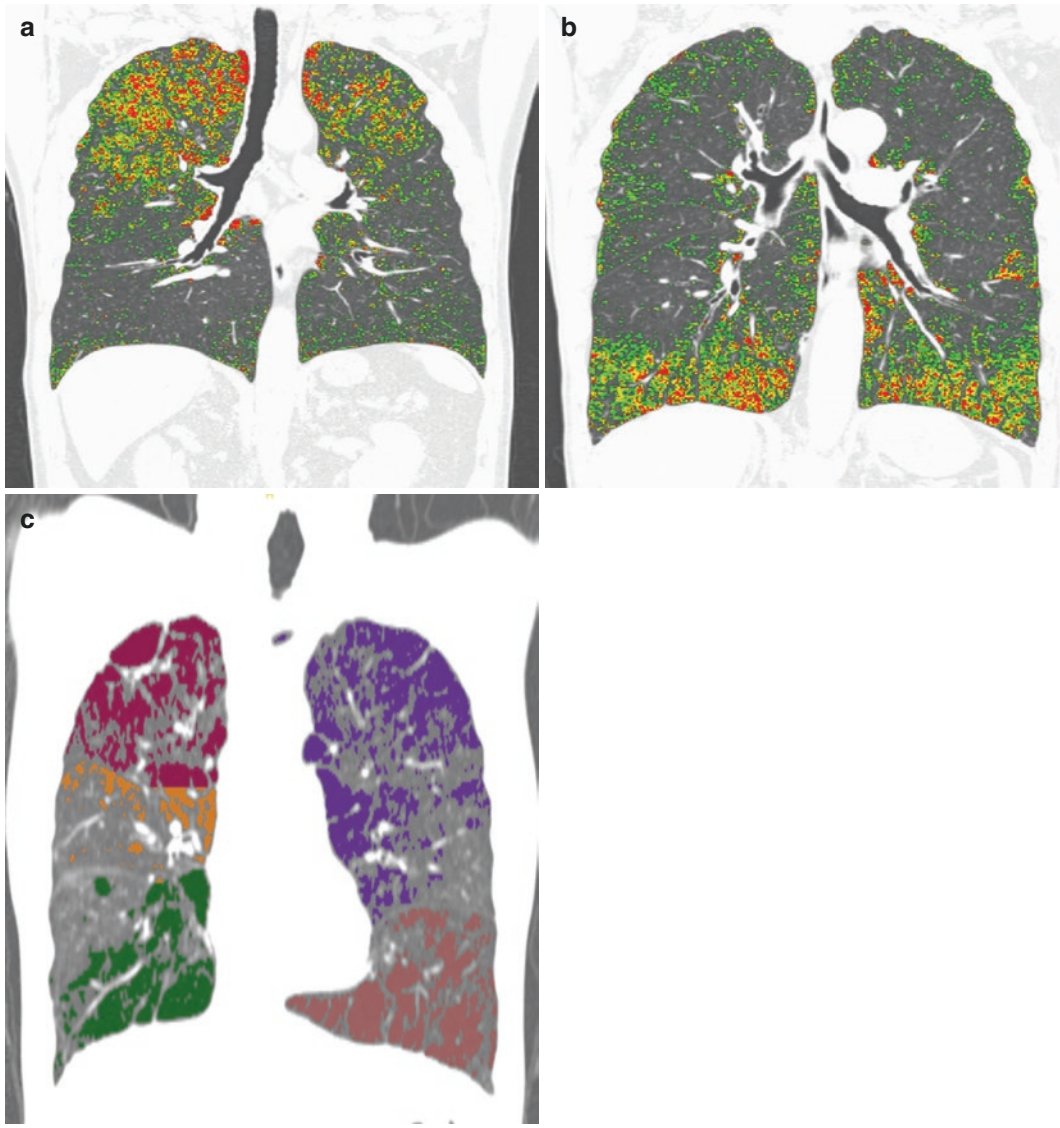

Fig. 8.10 Regional heterogeneity. CT images with color mapping (**a**, **b**) show different predominance of emphysema in two patients with similar emphysema index (17.56 and 23.27%). This regional heterogeneity can also be quantified by emphysema on each lobes (**c**)

is commonly found in heavy cigarette smokers with a sign of chronic bronchitis (Fig. 8.4). Bronchiectasis is also a common finding in COPD associated with severe airflow obstruction and risk for COPD exacerbation [14, 15, 35].

Airway Change: Computer-Based Quantification

With the current development of available software permitting multiplanar reconstruction of airways from thin-section volumetric datasets, CT scan seems to be well positioned to become the method of choice to noninvasively measuring airway wall dimensions of luminal diameter and wall thickness to the level of segmental and subsegmental airways. The simple analysis of "full-width at half maximum" algorithm is commonly used to evaluate the airways including absolute measures (bronchial luminal diameter or area, bronchial wall thickness or area, and total

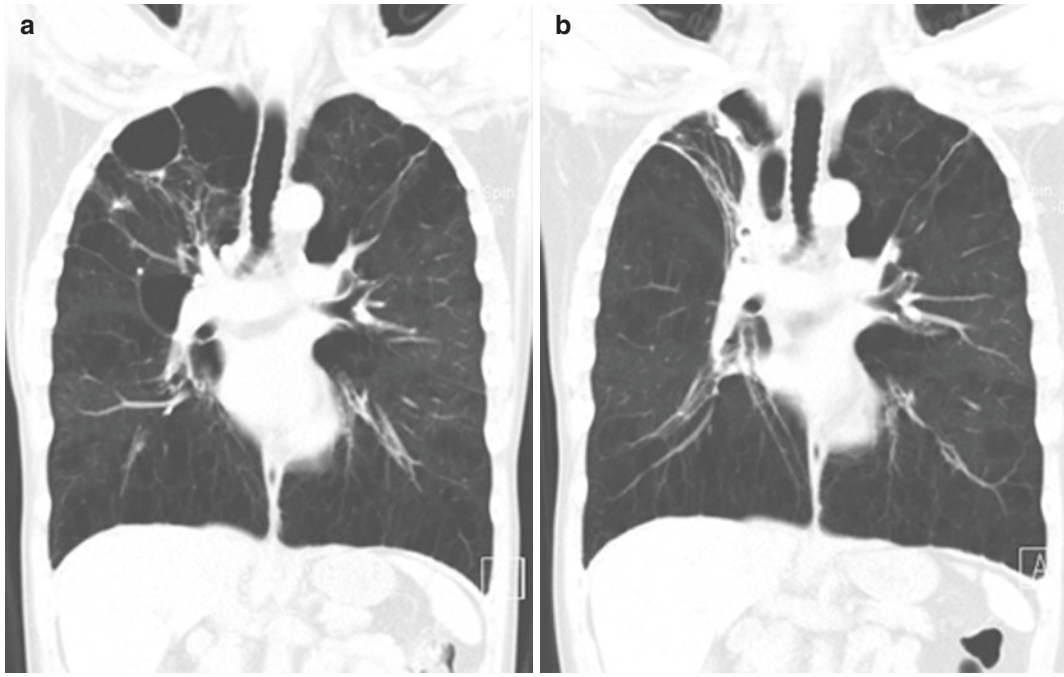

Fig. 8.11 Effect of lung volume reduction procedure. (**a**) CT image in a 61-year-old male showed severe and regional heterogeneity of emphysema. Endobronchial L was performed to collapse the RUL which was most severely affected by emphysema. (**b**) After the procedure, RUL was near totally collapsed on CT and pulmonary function of this patient much improved (FEV1, 0.46 L —> 0.82; mMRC, Gr4 —> 1)

bronchial area) and relative measures (bronchial wall area %, WA%: 100 × (wall area)/(lumen + wall area)) (Fig. 8.12). Variable software algorithms to define the boundaries of airway wall have been proposed and tested. Another commonly used measure is the square root of wall area of a hypothetical bronchus having internal perimeter of 10 mm (Pi10) [36].

Correlation Between Airway Measures and Clinical Parameters

Many studies showed that patients with the greatest WA% had the lowest FEV_1 expressed as a percent predicted [37]. The WA% has been considered as the most commonly employed metric for clinical investigation, and there are modest correlations between airway WA% and lung physiologic impairment [10, 38]. Moreover, central airway remodeling apparent on CT may reflect the distal histopathologic remodeling of the small airways, so the greater the central airway wall thickening, the more small the airway disease [39]. Moderate correlations ($-0.56 < r < -0.62$) between airway wall measurements and airflow obstruction (FEV_1 and FEV_1% predicted) have been reported and stronger correlations were noted when only small airways were analyzed [40]. In recent report, bronchial wall thickening as well as severity of emphysema measured on QCT is associated with exacerbation frequency, independently; bronchial predominant and emphysema predominant subtypes of COPD can be defined [41].

Other Large Airway Changes in COPD

Among the large airway changes in COPD, Saber-sheath trachea is not an uncommon finding in COPD (Fig. 8.5). It defines as the ratio of the sagittal to coronal diameter is greater than 2 and the extra-thoracic portion of the trachea is not narrowed. By comparison with normal healthy persons, COPD patients show that this tracheal morphologic change of the elongation of the sagittal diameter correlated with the severity of

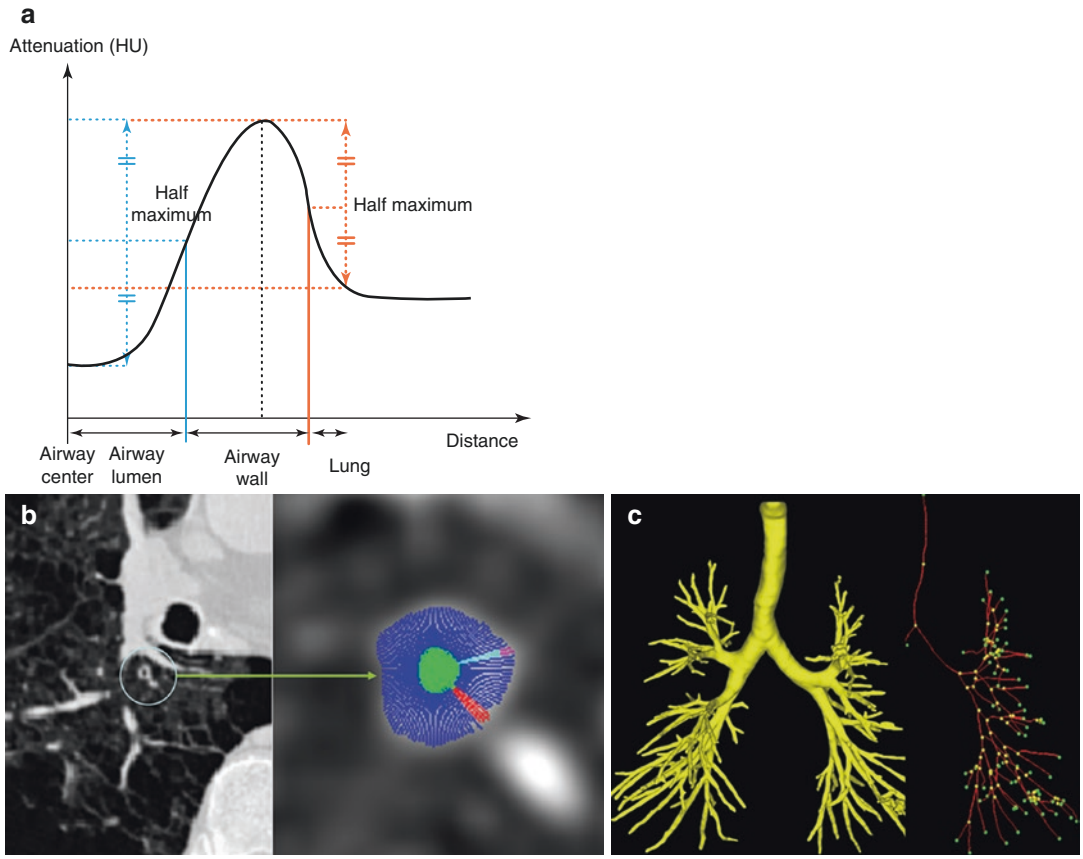

Fig. 8.12 Quantification of airway wall thickening using computerized method principle for full-width-at-half-maximum (FWHM) method. In the attenuation profile along an outward flowing ray from the luminal center-point through the airway wall, the inner and outer airway wall boundaries are assumed halfway to the maximum on the lumen side and halfway to the minimum on the parenchymal side, respectively. (**a**) After the detection of boundaries, the airway wall area can be highlighted with color overlay (**b**). This method is called as full-width-at-half-maximum method and is most common method to quantify wall thickness. The airway dimensions of the whole airway trees can be assessed using automatic airway segmentation, centerline extraction, followed by airway quantification (**c**)

emphysema and QCT indices, reflecting airflow limitation and air trapping [42]. Furthermore, expiratory tracheal collapse in obese COPD patients shows greater quality of life impairment and worse exercise performance than expected based on functional measures [43].

Small Airway Disease: Visual Assessment

The small airways are referred to as airway lumen less than 2 mm, those cannot be visualized using current CT scanners. The presence of air trapping on expiratory CT scan can be identified as an indirect sign to evaluate small airway remodeling. However, accurate discrimination between emphysematous area and air trapping area is difficult and challenging, and even normal healthy person can show minimal air tapping area in both basal lobes. Recently, there have been introduced several methods to evaluate the degree of pathologic air trapping in COPD patients using QCT.

Small Airway Disease: Computer-Based Quantification

With the usage of expiratory CT images, quantitative assessment of air trapping is possible.

However, there are severe inborn limitations when only expiratory CT is used because it is impossible to separate trapped air area from air remaining in emphysematous spaces. Moreover, air trapping phenomenon can also be seen in healthy smokers and healthy individuals with normal lung physiology. However, even with these drawbacks, many studies have evaluated the presence of air trapping in COPD by assessing the area fraction of the lung lesion having CT values lower than the threshold of −856 or −850 HU (LAA_{exp856} or LAA_{exp850}) in expiration [44]. With this simple method, they reported that high correlations were noted between LAA_{exp850} and FEV_1/FVC and FEV_1 percent predicted. As an effort to overcome this single threshold method of combining air trapping and emphysema quantification into single measure, quantifying air trapping outside the emphysematous area is possible through the density-based quantification method [45, 46]. With excluding emphysema portion of all voxels with attenuation lower than −950 HU from inspiration and expiration scans and calculating the relative volumes for whole lung with attenuation value less than −860 HU on each inspiratory CT (inspiratory relative $volume_{< -860\ HU}$) and expiratory CT (expiratory relative $volume_{< -860\ HU}$), the relative volume change between −860 and −950 HU can be calculated as follows: Relative volume change $_{< -860\ HU}$ (%) = expiratory relative $volume_{< -860\ HU}$ — inspiratory relative $volume_{< -860\ HU}$. Results from this method show that air trapping correlates with lung physiologic parameters significantly ($r = 0.50–0.80$). Other methods for measuring air trapping have been addressed as an index of air trapping including the ratio of inspiratory to expiratory lung volume ($E/I\text{-}ratio_{LV}$) and the expiratory to inspiratory ratio of mean lung density ($E/I\text{-}ratio_{MLD}$) [47, 48]. $E/I\text{-}ratio_{MLD}$ correlates with clinical parameters of COPD such as BODE-index ($0.48 < r < 0.68$) and $E/I\text{-}ratio_{LV}$ shows almost perfect correlation with $E/I\text{-}ratio_{MLD}$ ($r = 0.95$, $p < 0.001$). All of these values have a limitation that it can't represent regional distribution of air trapping. Recently, new approach of air trapping assessment has been proposed [49, 50]. By using software techniques, anatomical correspondence of lung region between inspiration and expiration CT images can be assessed and both images can be co-registered. By direct assessment of density difference between inspiration and expiration CT, the density change map can be generated and the areas with decreased density change can be defined as the area of air trapping. By using this method, in addition to the global assessment, regional assessment of air trapping is possible (Fig. 8.13) [49, 50].

Other Components of COPD: Correlation with Clinical Parameters

Texture-Based Emphysema Assessment

With an effort to discriminate various obstructive lung diseases from normal lung, more sophisticated automatic classification system based on the texture and shape features of CT images has been introduced. Using this method, further differentiation of lung areas, for example, into normal lung, small airway disease, centrilobular emphysema and panlobular emphysema, is possible. This quantification method showed comparable correlation with the pulmonary function test results when compared with conventional density-based quantification [51, 52]. This method can also be used for the assessment of combined pulmonary fibrosis.

Pulmonary Vascular Change

Pulmonary vascular change is also one of the characteristic features of COPD and the extent of emphysema, rather than airway obstruction, is responsible for pulmonary endothelial dysfunction in COPD [53]. After volumetric CT scans of the lung, pulmonary vasculature was automatically segmented from the parenchyma using software [54, 55] (Fig. 8.14). With the usage of QCT measuring the cross sectional area (CSA) of small pulmonary vessels (sub-subsegmental level, CSA less than 5 mm^2), the total CSA of small pulmonary vessels in COPD shows strong (negative) correlation with the extent of emphysema ($\%LAA_{-950}$), whereas weak correlation with airflow obstruction [56]. The anatomic extent of emphysema instead of airway obstruction is responsible for impairment of pulmonary

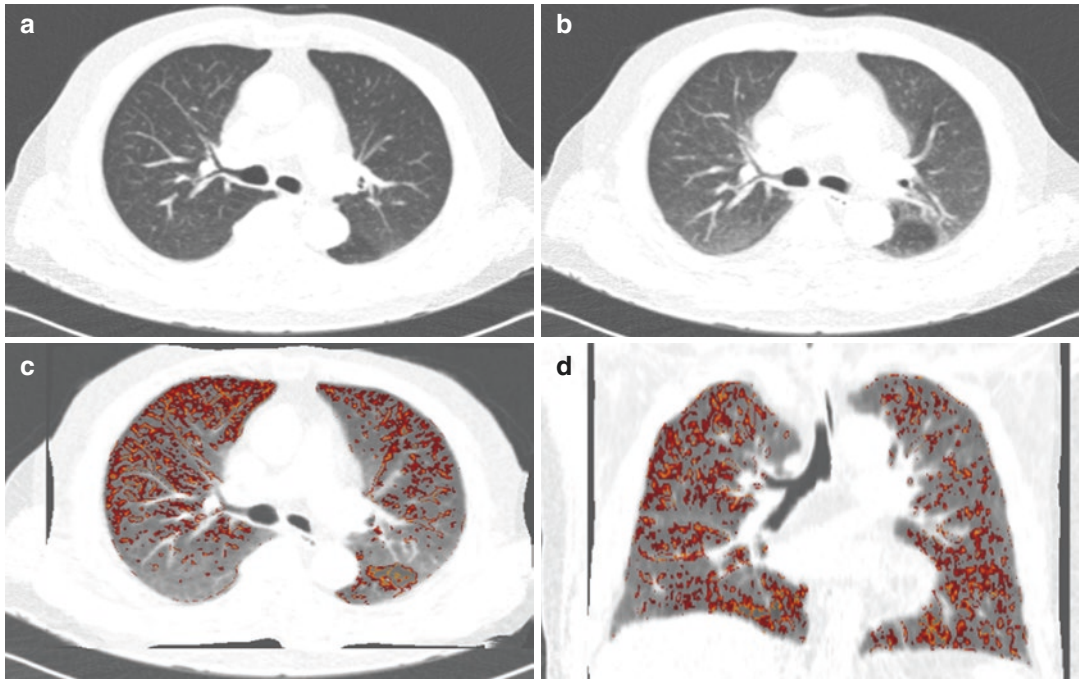

Fig. 8.13 Subtraction image from co-registered inspiratory and expiratory images. Image maps (**c**, **d**) derived from co-registered inspiratory (**a**) and expiratory (**b**) images depict changes in lung attenuation from inspiration to expiration. Using image registration technique, the expiration CT image is deformed to match with the corresponding anatomical area on inspiration CT (**c**). By comparing CT attenuation between inspiration CT and registered expiration CT, area of air trapping with little change in CT attenuation can be extracted and visualized in color overlay (**c**). This process is applied in the whole lung and coronal distribution of air trapping can be visualized (**d**)

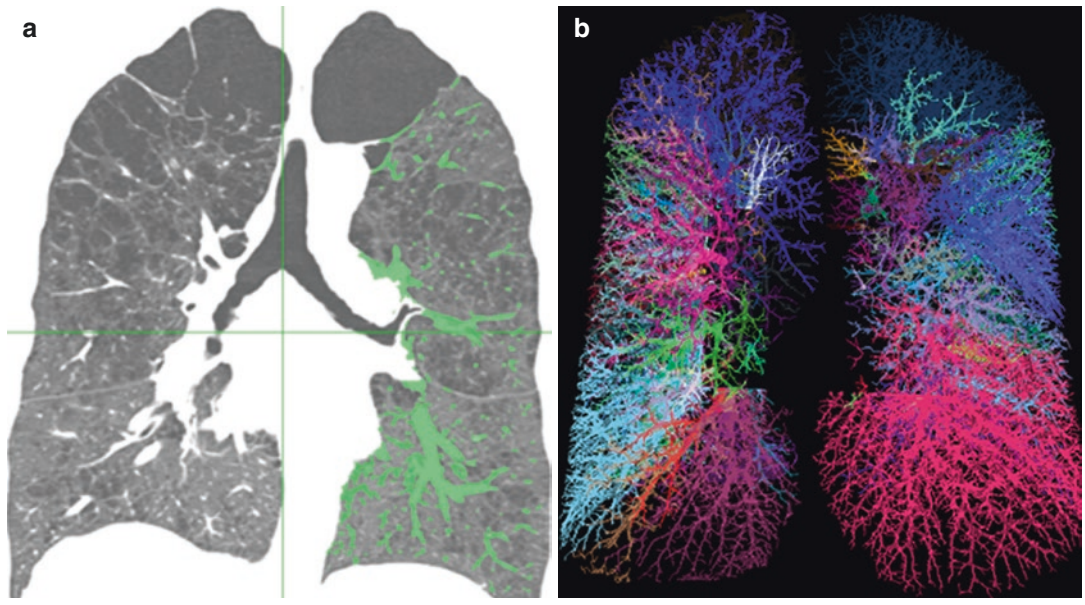

Fig. 8.14 Vascular subbranches of lung. (**a**) Extraction vessels in CT and (**b**) Vascular tree reconstruction; random coloring; each color represents one vascular branch and mediastinal region is cropped

vascular structure. Moreover, the percentage of the total CSA for the lung area is significantly higher in airway dominant phenotype than emphysema dominant phenotype.

Osteoporosis

Osteoporosis should be considered as one of the important pathology of COPD, because it may cause vertebral compression fractures, which can also deteriorate FEV_1 and decrease in vital capacity. Actually, the loss of vertebral bone mineral density on CT is closely related to the severity of emphysema showing many risk factors of low BMI, decreased activity, systemic inflammation, and use of corticosteroids [17, 57, 58] (Fig. 8.15). There has been reported that the decrease in thoracic vertebral bone mineral density is greater in patients with a history of exacerbations than in those without a history of exacerbations. Indeed, osteoporosis progression should be checked in COPD patients, especially in those with a history of frequent exacerbations [59].

Chest Wall and Diaphragm

COPD is also characterized by progressive impairment of respiratory function and dysfunction of respiratory muscle. There have been reports that the depletion of peripheral muscle mass is a better predictor of mortality than BMI in patients with COPD [60, 61]. Thoracic respiratory muscles are unique and crucial for alveolar ventilation and weakness of respiratory muscle results in dyspnea and respiratory failure associated with mortality in COPD patients. It is reported that intercostal mass and intercostal attenuation measured by QCT are significantly correlated with FEV_1 and extent of emphysema of QCT measurement [62]. A decrease in thoracic muscle mass with increasing intercostal fat is associated with worsening of COPD (Fig. 8.16). Hyperinflation in COPD makes diaphragm to be flatter and shorter. As the progression of COPD, breathing becomes gradually more dependent on the thoracic intercostal muscles than diaphragm (Fig. 8.7).

Atherosclerosis

In COPD patients, reduced FEV_1 has known to be an increased risk factor for cardiovascular diseases and mortality, independent of smoking [63, 64]. In other words, systemic inflammation in COPD patients may accelerate the rates of cardiovascular disease, and this degree or status of atherosclerosis may be associated with impaired lung function and emphysema in COPD patients. There has been an attempt to demonstrate the

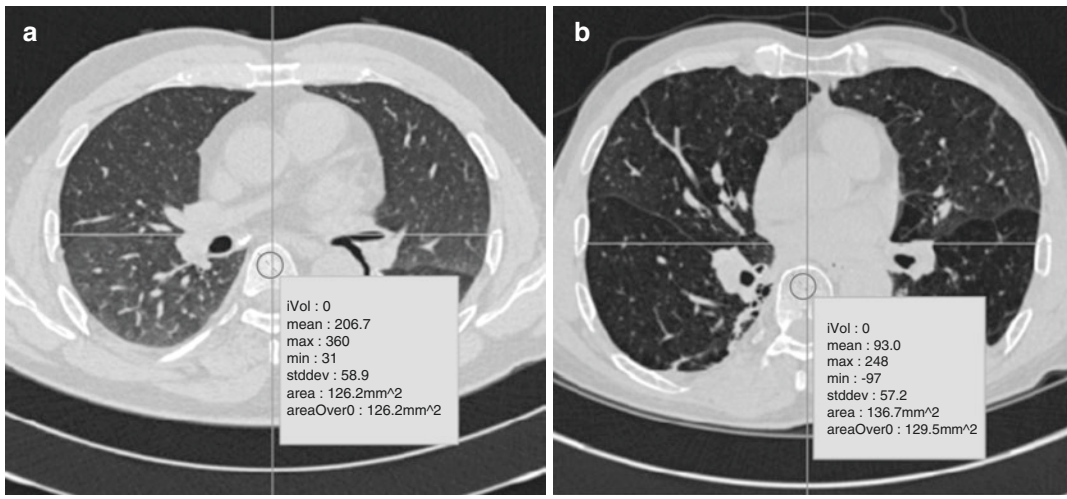

Fig. 8.15 Thoracic bone density on CT image. Vertebral bone mineral density on CT is closely related to the severity of emphysema. (**a**) CT image of a 59-year-old male with 6.2% of emphysema index shows 206.7 HU on thoracic vertebra. (**b**) CT image of a 79-year-old male with 52.2% of emphysema index shows 93.0 HU on thoracic vertebra

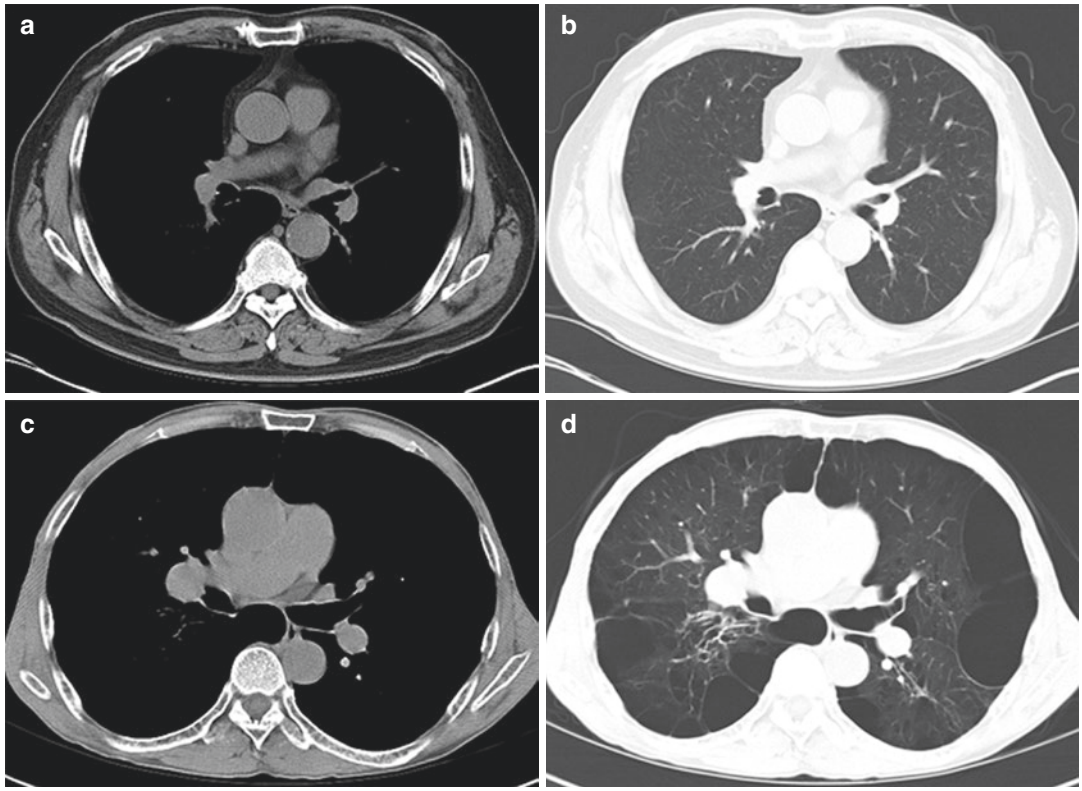

Fig. 8.16 Thoracic muscle mass on CT image. Thoracic muscle mass and intercostal fat are associated with severity of COPD. (**a**, **b**) CT images of a 75-year-old male with 7.4% of emphysema index shows more prominent thoracic muscle mass than CT images of a 62-year-old male with 54.8% of emphysema index

association of the total amount of calcification in coronary artery, thoracic aorta, mitral and aortic annuli, and the extent of emphysema on QCT and lung physiology [65]. Calcium score as a measurement for degree of atherosclerosis shows weak but significant correlation with volume fraction of emphysema on QCT, FEV_1/FVC, and diffusion capacity, independent of age, BMI, and smoking amount. The degree of atherosclerosis is associated with impaired lung function and the extent of emphysema.

Imaging Studies of Treatment Monitoring and Disease Progression

Predicting Tool in Treatment Outcome

COPD is a heterogeneous condition featuring both parenchymal destruction (emphysema) and small airway disease (obstructive bronchiolitis); its relative contributions vary in each COPD patient. Previous studies already have suggested that different spirometric response patterns to bronchodilator exist in patients with obstructive lung disease showing improvement in expiratory flow (FEV_1) or lung volume (FVC) [66, 67]. Therefore, QCT measurements can be used as a longitudinal evaluation of treatment monitoring based on the fact of a significant correlation between QCT measurement indices and lung physiologic indices. Notably, in the assessment of different spirometric response patterns to bronchodilator treatment, the extent of emphysema in QCT measurement shows a significant negative correlation with postbronchodilator FEV1 change and the E/I-$ratio_{MLD}$ also shows a significant positive correlation with postbronchodilator FVC change [68]. In case of lung volume reduction therapy in regions with severe emphysema, QCT can be used as a predictor of

improvement of lung function after surgical or bronchoscopic approaches [34].

Disease Progression

There have been several efforts to evaluate the progression of emphysema using QCT measurement and QCT is useful in demonstrating the change in extent of emphysema directly (Fig. 8.17). However, the main drawback of QCT measurement is a variation of inspiration level on each CT scan. Studies showed that the change in the 15th percentile CT density after the correction of lung volume difference was found to be more sensitive as an index of progression compared with measures of physiology or healthy status [69]. Recently, new single unified approach using a voxel-wise imaging analysis can be used in diagnosing disease extent and phenotype of COPD, detailed spatial distribution and location. This method allows us to distinguish the relative contributions of functional small airway disease component and emphysema in COPD in the course of disease progression [49].

Quality Control and Standardization

Emphysema Quantification

There are several sources of variation in quantification of emphysema in COPD including scanner, software, and patient factors. Thinner slice thickness and the lower CT dose setting result in overestimation of emphysema extent on QCT due to increasing image noise [4]. Inter- and intra-scanner variation due to calibration error and beam hardening effects should also be considered, and there have been attempt to demonstrate that density correction of volumetric CT

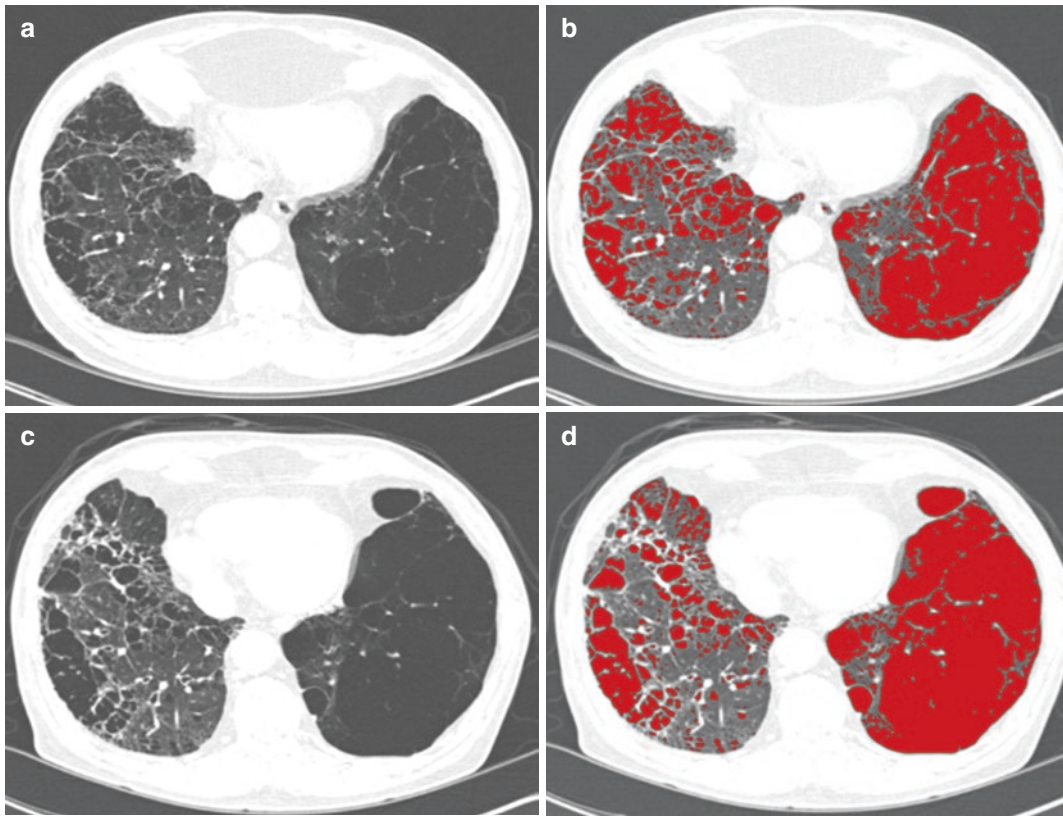

Fig. 8.17 Follow-up emphysema quantification (LAA, %) in same subject. Initial emphysema index (EI, %) was measured to 41.8% on CT image (**a**) and matched color coding image (**b**). Three years hence, EI has increased and measured to 56.2% on CT image (**c**) and matched color coding image (**d**)

data based on air (reference value: −1000 HU in tracheal air or outside patient air) will improve the correlation between emphysema quantification and pulmonary function test [70, 71]. This correction method may be useful to decrease the variation of measured results when multiscanners are involved. Second, a smooth reconstruction algorithm is usually recommended for the emphysema quantification using QCT because a strong or overenhancing algorithm can result in overestimation of emphysema [6]. Regarding patient factors, variation in lung volume, which is influenced by degree of inspiration, can be a major source of variation in clinical practice. Measurements of emphysema can be different at varying inspiration levels. However, quantitative measurement of differences in emphysema would not be significant when scans are obtained above 90% of vital capacity [72]. Current smoking status or coexisting air trapping or parenchymal fibrosis can also alter the quantitative emphysema measurements. Measured extent of emphysema in current smokers appears to be lower than those in former smokers, probably due to increased attenuation induced by smoking-related infiltration of inflammatory cells in the lungs in current smokers [73, 74]. Therefore, for accurate and precise quantitative assessment of emphysema extent, it is important to consider and control all the factors discussed above.

Airway Quantification

In quantitative airway measurements, considering factors about the source of variation are similar to emphysema measurements. Because airway is small, it is easily influenced by partial volume averaging and reconstruction algorithm than in quantitative measurement of emphysema. Appropriate radiation dose to overcome image noise during reconstruction and submillimeter section will reduce the variation in airway measurements. In addition, there are varieties of suggested software algorithms to measure airway dimension, resulting in different measurement values. Accordingly, usage of same software method is essential in multicenter trial or for following up the patients.

Magnetic Resonance Imaging (MRI)

The MRI can obtain morphologic and functional imaging without ionizing radiation. However, there are some reasons of difficulty in imaging the lung with MRI. The lung consists of the low density tissue, so it contains a relatively small number of protons which generate signal in MRI. In the lung, these are fast decay of signal due to susceptibility artifacts from countless air-tissue interfaces. The fast imaging, triggering, and gating techniques are needed due to respiratory, vascular, and cardiac motions. The major advantage of MRI is combination of morphological and functional lung imaging, such as perfusion, ventilation, blood flow, gas exchange, and respiratory motion, with high spatial and temporal resolution [75].

Morphologic Evaluation of COPD

Simply speaking, there are two different types in COPD. The airway type relates to chronic bronchitis and airflow obstruction. The emphysema type shows the parenchymal destruction with severe airflow obstruction and distal airspace enlargement. The morphologic evaluation in COPD using MRI is always compared to CT. MRI is technically more challenging due to hyperinflation and loss of lung tissue [76]. So, there are only a few publications on morphologic evaluation of COPD using MRI.

Imaging Technique

Many MRI sequences can be used for visualization of the lung: balanced steady-state free precession (bSSFP), volumetric interpolated breath-hold examination (VIBE), half-Fourier-acquired single-shot turbo spin-echo (HASTE), and ultra-short echo time (UTE) [77–79]. Three-dimensional (3D) T1-weighted gradient-echo sequences are used for the assessment of mediastinum and lung parenchymal tissues. T2-weighted fast spin-echo with half-Fourier acquisition sequence can visualize bronchial wall thickening and mucus plugging. Respiratory, vascular, and cardiac motions can be overcome by using fast

imaging, gating, and triggering techniques. Half-Fourier acquisition or ultra-short echo times are recommended.

Emphysema

It is a major role of T1- and T2-weighted images to differentiate inflammation from muscular hypertrophy, edema, and mucus plugging in bronchial wall [80]. Emphysematous change of lung cannot be easily diagnosed by a loss of signal. However, hyperinflation can be easily detected by increased lung volume and reduced blood volume. There is one study about the change of signal intensity of lung parenchyma between inspiration and expiration MRIs, which is correlated with FEV_1 [81]. The MR signal can be improved and emphysema can be quantified by using the UTE pulse sequences [82]. Using fast radiofrequency (RF) excitation pulses, compressed sensing and parallel imaging in UTE pulse sequence, MR signal decay, and motion artifacts can be minimized [83]. UTE pulse sequences improve contrast-to-noise ratio, signal-to-noise ratio, and signal intensity with strong relationship between signal intensity and tissue density. Using UTE pulse sequence, pulmonary emphysema [84, 85], lobar fissures and airways [86], inflammation and peribronchial abnormalities [87] can be estimated.

Airway

There are several factors, such as bronchial level, diameter, wall thickness, and signal from bronchus, to detect bronchiectasis [88]. MRI usually visualizes central and peripheral bronchiectasis and central bronchi, whereas poorly visualizes normal peripheral bronchi. Using 3D volume interpolated gradient-echo sequence (VIBE) with high spatial resolution, the airway can be visualized [89]. T2-weighted sequences can visualize inflammation, mucus, edema, and fluid collections. Active inflammation can be represented by increased fluid, which shows high signal of the bronchial wall on T2-weighted sequences. Inflammatory activity has relation with contrast enhancement of thickened bronchial wall on contrast-enhanced T1-weighted sequence. Therefore, airway inflammation can be visualized by high signal on T2-weighted and contrast-enhanced T1-weighted sequences [90]. In contrast, mucus plugging on peripheral bronchi shows high signal intensity of fluid content on T2-weighted sequence without contrast enhancement on T1-weighted sequence on MRI.

Perfusion MRI

Using perfusion MRI, perfusion information of lung can be acquired without ionizing radiation. One of the advantages using perfusion MRI in COPD is combination of perfusion and morphologic information about parenchymal destruction and cause of perfusion changes. Several imaging techniques have been introduced.

Imaging Techniques

For assessment of pulmonary vasculature and perfusion, both of non-contrast-enhanced and contrast-enhanced sequences are available. Non-contrast-enhanced perfusion MRI can be acquired using arterial spin labeling technique, which is to mark a specific part of spins magnetically using radiofrequency (RF) excitation [91]. Using the electrocardiogram (ECG) gating technique, signal differences between systolic phase and diastolic phase can make perfusion images of the lung without contrast injection [92]. However, one of the limitations of ECG-gated perfusion MRI is that the image subtraction process is sensitive to misregistration due to bulk respiratory motion [91]. Contrast-enhanced 2D and 3D MRI, which is based on dynamic acquisition of lung tissue during contrast injection, can assess lung perfusion and quantify pulmonary perfusion [93, 94]. The advantage of contrast-enhanced perfusion MRI is high signal-to-noise ratio [95]. For evaluation of whole lung perfusion during peak enhancement period, 3D technique should be needed. For improvement of spatial resolution and reduce of the total acquisition time, k-space sampling techniques such as parallel imaging techniques or echo sharing techniques can be used [96, 97].

Quantification

Using MR perfusion technique, pulmonary blood flow can be assessed quantitatively [98, 99]. The indicator-dilution theory using the maximum of signal intensity and the temporal course of the signal change is base of quantification of pulmonary perfusion. If linear relation can be assumed between the concentration of contrast agent and the signal, concentration-time curves can be made by conversion of signal-time curves. The relationship among the perfusion parameters—pulmonary blood flow (PBF, mL/100 mL lung tissue/min), pulmonary blood volume (PBV, mL/100 mL lung tissue), and mean transit time (MTT, s0) is as follows:

$$MTT = \frac{PBV}{PBF}$$

Normalizing the area under the tissue concentration-time curve to the integral of the arterial input function can calculate PBV. Figure 8.18 shows quantification images of lung perfusion using perfusion MRI technique.

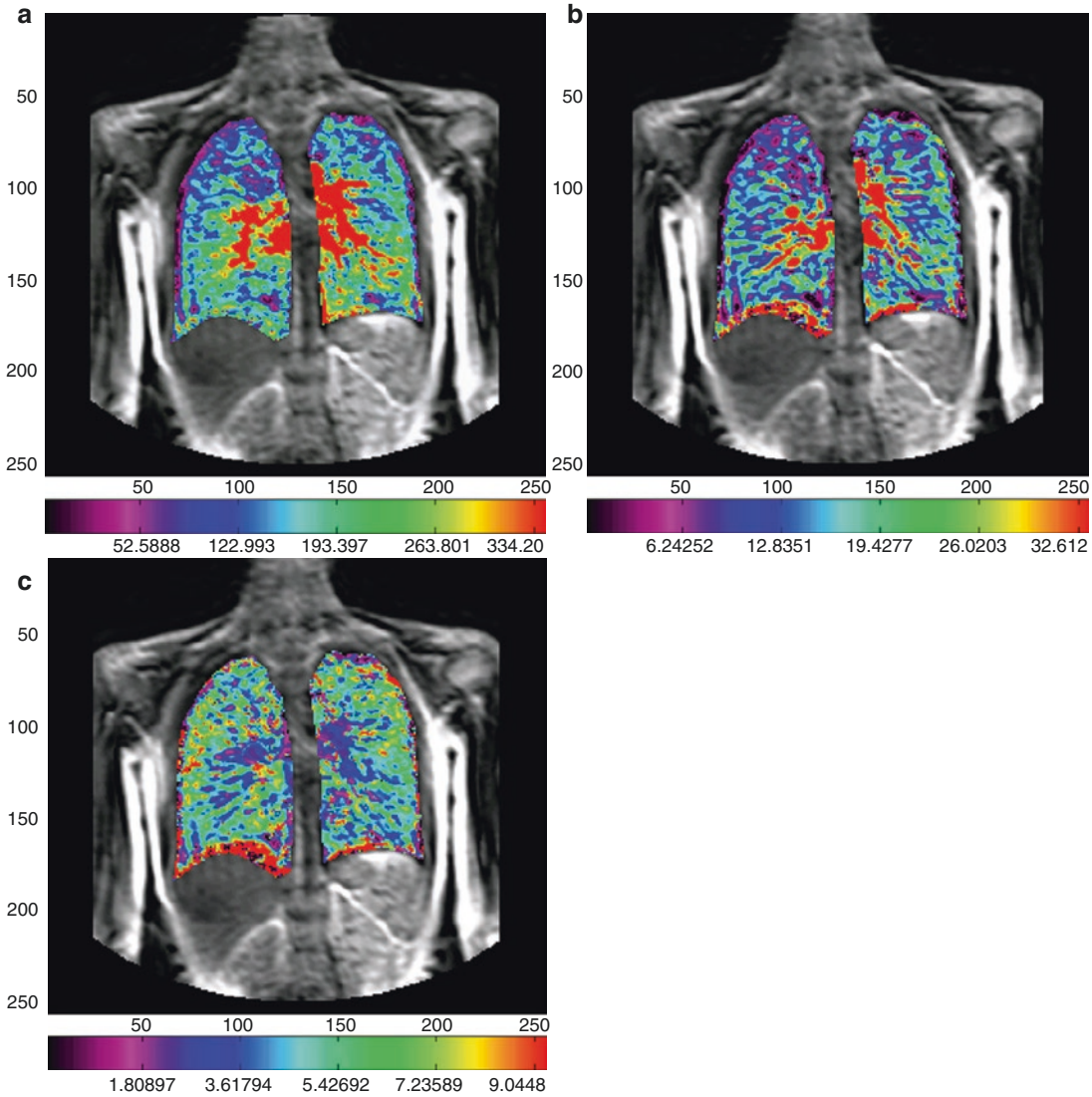

Fig. 8.18 Lung perfusion quantification image. Using perfusion MRI technique, PBF map (**a**), a PBV map (**b**), and an MTT map (**c**) are generated

COPD Studies Using Perfusion MRI

In COPD, chronic inflammation is thought to lead to intimal wall thickening and smooth muscle hypertrophy of pulmonary arteries. Hyperinflation and air trapping can make hypoxic vasoconstriction. Perfusion MRI shows high accuracy in detecting perfusion abnormalities in patients with emphysema [100, 101]. The perfusion abnormalities in COPD usually show a low degree of inhomogeneous contrast enhancement, especially in the area of severe emphysema [102] and decreased peak signal intensity. In COPD patients with severe emphysema, visual assessment of perfusion using 3D perfusion MRI shows high agreement with parenchymal destruction [103]. With quantitative analysis, decreased perfusion parameters on MRI correlate with worsening of FEV_1/FVC and increased emphysema index on CT [104]. Quantitative perfusion MRI in COPD shows decreased value and heterogeneous change in mean pulmonary blood flow (PBF), pulmonary blood volume (PBV), and mean transit time (MTT) than those in normal volunteer [105].

Ventilation MRI

For assessment of lung ventilation, several methods of MRI, such as oxygen-enhanced MRI and hyperpolarized noble gas MRI, are developed. Repeated or time-resolved measurements of lung dynamics can be obtained using ventilation MRI.

Oxygen-Enhanced MRI

Oxygen-enhanced MRI can visualize lung ventilation. Oxygen couples to hemoglobin and is present as dissolved oxygen in blood during oxygen exchange between capillary beds and alveoli [106]. Paramagnetic property of deoxyhemoglobin makes little T1 shortening effect with T2* shortening effect [107, 108]. Dissolved oxygen makes shortening of T1 relaxation time of blood in pulmonary vein due to paramagnetic property of oxygen [107]. This shortening leads to increased signal intensity on oxygen-enhanced MRI [109, 110]. Several sequences, such as centrically reordered phase-encoding scheme on HASTE sequence and single-shot rapid acquisition with relaxation enhancement (RARE) or HASTE sequences, can make oxygen-enhanced MRI [111]. Respiratory gating techniques are preferred because pulmonary physiology and physiopathology can be affected by breath hold despite decreased misregistration. Oxygen-enhanced MRI is used to assess ventilation abnormalities in pulmonary emphysema [112]. Regional changes in ventilation on oxygen-enhanced MRI reflect the regional lung function [113]. Figure 8.19 shows ventilation of patients with severe COPD using dynamic oxygen-enhanced MRI. FEV_1 and DLco well correlate with slope of oxygen-enhancement time-course curve and degree of oxygen-enhancement, respectively. Dynamic oxygen-enhanced MRI reflects DLco and provides diffusing capacity maps [112].

Hyperpolarized Noble Gas MRI

Using hyperpolarized noble gas MRI with ^{3}He or ^{129}Xe gas, ventilation MRI can be acquired [110, 114, 115]. These techniques visualize the ^{3}He or ^{129}Xe gas in airway and airspaces, so it can be used for regional mapping of airflow and assessment of diffusion in airspace [116, 117]. For these techniques, specialized laser equipment and specialized RF transmitter and receiver coils are mandatory. Four different techniques are used for hyperpolarized ^{3}He MRI [118]. Static ventilation imaging generally uses 2D or 3D fast low-angle single-shot or bSSFP sequences [119]. Diffusion imaging uses gradient-echo pulse sequence with bipolar diffusion-sensitizing gradient waveform between the excitation RF pulse and data acquisition [120]. Dynamic ventilation imaging uses the ultrafast pulse sequences such as interleaved spiral pulse sequence with good balance between spatial and temporal resolution [121]. Oxygen partial pressure imaging uses the paramagnetic effect of oxygen on polarization of ^{3}He [122]. Single-acquisition and single breath-hold technique improves temporal resolution and reduces error due to second breath hold. MRI with this technique can directly measure the regional ventilation and perfusion distribution [123]. Because ^{129}Xe is naturally richer than ^{3}He

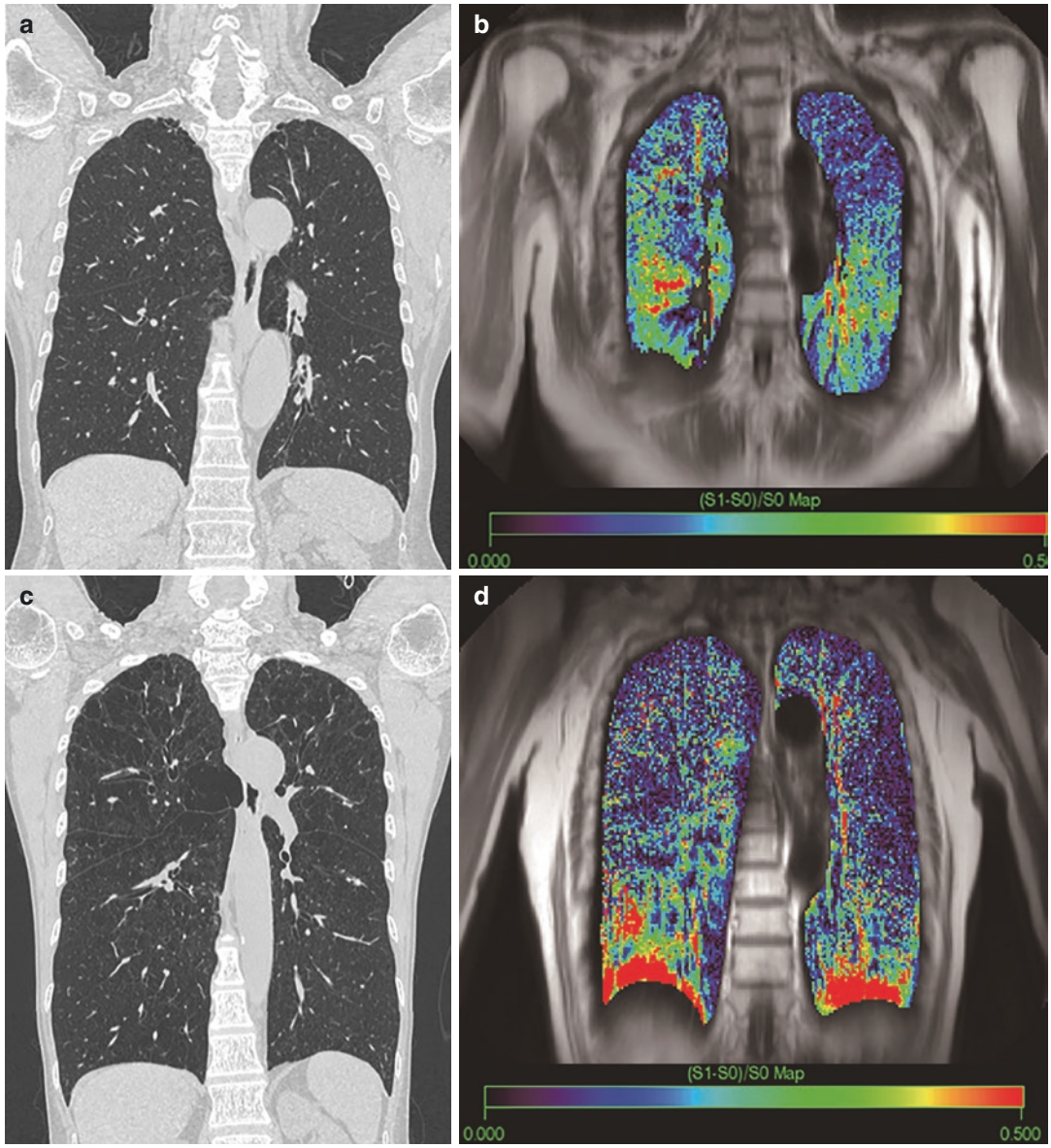

Fig. 8.19 Oxygen-enhanced MRI in COPD patients. (**a**, **b**) A 75-year-old female smoker with mild COPD (**a**: thin-section coronal multiplanar reformatted (MPR) CT image shows centrilobular emphysema in the left upper lung field, **b**: relative enhancement (RER) map from oxygen O_2-enhanced MRI demonstrates heterogeneously decreased oxygen-enhancement in the both lung, especially left upper lung filed.) (**c**, **d**) a 56-year-old female smoker with severe COPD (**c**: thin-section coronal MPR CT image demonstrates panlobular emphysema in bilateral upper and middle lung field. **d**: RER map from oxygen O_2-enhanced MRI demonstrates heterogeneously decreased oxygen-enhancement in the both lung, especially upper lung fields.) Image courtesy of Yoshiharu Ohno, Kobe University Graduate School of Medicine

and ^{129}Xe MRI shows comparable quality to ^{3}He MRI with recent advances in polarization and imaging methods; many methods of ^{3}He are translated for ^{129}Xe. However, ^{129}Xe MRI differs from ^{3}He MRI due to difference of gas distribution. In stage III COPD, ventilation defect volume (VDV) was sensitive to minimal changes during short-term follow-up [114]. Percentage of

ventilation volume was significantly different among three groups (healthy volunteers, healthy asymptomatic smokers, and COPD patients). COPD patients are separated from healthy subjects by apparent diffusion coefficient (ADC) map [124]. Using diffusion-weighted hyperpolarized ^{129}Xe MRI, ADC was significantly correlated with PFTs (FEV_1, FEV_1/FVC, and DLco) [115]. Ventilation defect percentages in ^{3}He MRI show significant correlations with ventilation defect percentages in ^{129}Xe MRI and ventilation defect percentages show strong correlations with FEV_1 [125]. ADC can measure airspace size sensitively. In COPD, airspace dimensions are increased compared to non-smokers [126]. ADCs in emphysema show regional variations and significantly larger than those of healthy volunteers, which is homogeneous [127].

Fourier Decomposition MRI for Combined V-Q Imaging

Non-contrast-enhanced ventilation and perfusion MRI, known as Fourier decomposition MRI, uses a short echo dynamic SSFP acquisition with subsequent compensation for respiratory motion by using non-rigid image registration [128, 129]. Peaks at the respiratory and cardiac frequencies can be identified by spectral analysis of the image time series. Deformation of lung parenchyma and pulmonary blood flow leads to regional proton density change, which is related to amplitude of these peaks [130]. With image post-processing, ventilation- and perfusion-weighted maps are generated for regional assessment of lung function from a single acquisition series [131].

Dynamic Respiration MRI

Diaphragmatic geometry is affected by hyperinflation of the lung. Dynamic respiration MRI with fast-acquisition technique can visualize complex interaction between chest wall and diaphragmatic motion with high spatial and temporal resolution [132]. Using dynamic respiration MRI, the change in lung volume during the respiratory cycle can be assessed. In emphysema patients, motion of the diaphragm and chest wall is reduced, irregular or asynchronous [133]. Emphysema in lower lung shows significant correlation with diaphragmatic flattening, abnormal chest wall motion, and severe airflow limitation [134]. Although both normal and paradoxical diaphragmatic motion is restricted by severe hyperinflation, the paradoxical diaphragmatic motion shows significant correlation with hyperinflation [135].

Other Imaging for COPD

Dual-Energy CT

Introduction of Dual-Energy CT

Dual-energy CT refers to CT that uses two different energy spectra (usually 80 and 140 kVp). With the knowledge about the X-ray attenuation change of a particular substance at two different X-ray energies, the material differentiation and elemental decomposition of tissues are possible in dual-energy CT [136, 137]. Therefore, with single contrast CT scanning at two different energies, the CT images used for structural evaluation are created by combination of the CT images from the low- and high-energy CT data, and the material-specific images such as iodine map or xenon map for functional evaluation are created by the material-decomposition algorithms in the postproccessing of dual-energy datasets (Fig. 8.20). Three different designs of dual-energy CT for the acquisition of dual-energy data have been proposed. Firstly, dual-source CT system has two separate X-ray tubes and two corresponding detectors, which are placed with an angular off-set of 90° on the rotating gantry. Each X-ray tube can be operated at different kilovoltage and milliamperage settings. Secondly, in rapid kVp switching, the single X-ray source is used and X-ray tube electronically switches the tube voltage between higher energy and lower energy in about 0.5 ms. Lastly, the energy-sensitive sandwich detector is now commercially available. This system uses a layered detector and single X-ray tube with the polychromatic

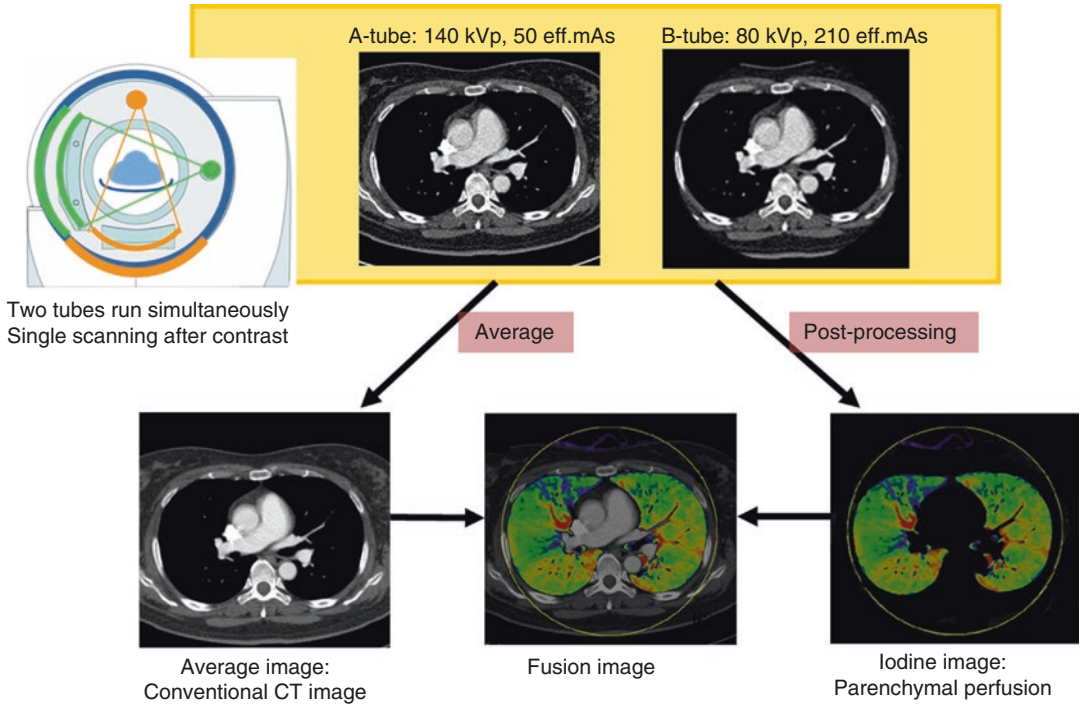

Fig. 8.20 Iodine perfusion imaging using dual-source CT. CT image data is generated in dual-energy acquisition mode of dual-source CT. Axial CT image is obtained at 140 kVp and 50 mAs from A-tube and at 80 kVp and 210 mAs from B-tube. And conventional CT image (approximate 120 kVp image) is generated from combination of the 140 and 80 kVp datasets. Iodine image is obtained with extraction of iodine component with material-decomposition theory in post-processing. Fusion image with conventional CT image and iodine image is generated for the evaluation of lung parenchymal perfusion

spectrum. The layered detector comprises two layers: a thin top scintillator that absorbs low energy photons and a bottom scintillator that absorbs the higher mean energy photons.

For COPD patients, which is characterized by airway obstruction and emphysematous alveolar destruction, pulmonary vascular changes are also produced, which are characterized by hypoxic vasoconstriction, numeric reduction, and endothelial dysfunction of the small pulmonary arteries [138–140]. These characteristic anatomic changes influence and impair alveolar gas exchange, and the uneven distribution of alveolar ventilation and pulmonary blood flow (V/Q mismatch) is the most important cause of arterial hypoxemia in the COPD patients [141, 142]. Therefore, evaluating COPD patients should focus on not only the extent and severity of anatomic destruction of the lung parenchyma but also the functional changes and impairment such as alveolar ventilation changes or parenchymal perfusion changes.

Perfusion Dual-Energy CT

Dual-energy CT-derived iodine map represents the iodine content of the capillary bed, i.e., pulmonary blood volume at the time of CT scanning rather than pulmonary blood flow. However, it has been demonstrated that the similarity of the dynamic CT-derived pulmonary blood flow and dual-energy CT-derived pulmonary blood volume [143]. Therefore, pulmonary blood volume, assessed with dual-energy CT, can be used for the evaluation of lung perfusion as a surrogate for dynamic CT-derived pulmonary blood flow with simpler protocol while maintaining quantitative similarity (Fig. 8.21).

In COPD, the regional lung perfusion impairment occurs due to the hypoxic vasoconstriction of the area with decreased ventilation

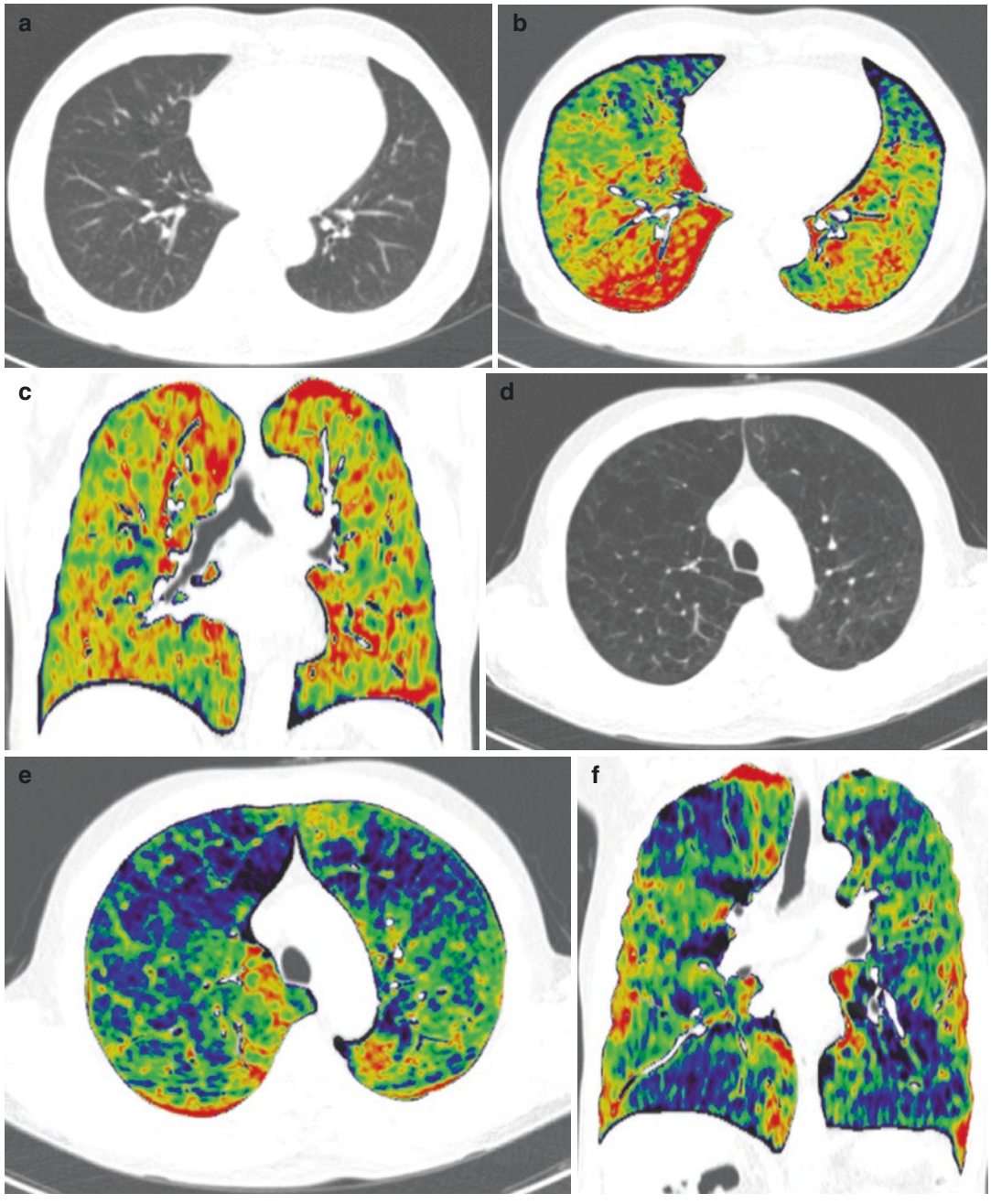

Fig. 8.21 Iodine perfusion image with dual-energy CT in COPD patient. (**a**–**c**) Dual-energy CT in COPD patient with mild emphysema. (**d**–**f**) Dual-energy CT in COPD patient with severe emphysema. From iodine perfusion CT using dual-energy CT, (**a**, **d**) weighted conventional CT image and (**b**, **c**, **e**, **f**) iodine perfusion map are generated. Lung parenchymal destruction in COPD patient can be assessed on high-resolution conventional CT image (**a**, **d**), and anatomically matched parenchymal perfusion information can be evaluated on perfusion map (**b**, **c**, **e**, **f**). In the area of confluent emphysema of both lower lobes, parenchymal perfusion is decreased (displayed with *blue color*)

and reduction of the pulmonary capillary by the chronic inflammation of pulmonary artery [144]. Moreover, alveolar surface destruction is accompanied by the reduction of the pulmonary capillary bed. Thus, considerable attention has been paid to the evaluation of lung perfusion alterations in COPD patients because the severity of parenchymal destruction and the alteration of lung perfusion determine the functional effect of emphysematous changes. Lung parenchymal perfusion has been assessed by perfusion scintigraphy, single-photon emission CT and MR. However, the distribution of perfusion impairment does not match with the area of parenchymal destruction [145]. Dynamic multi-detector CT perfusion imaging also can provide the regional perfusion. It has been demonstrated that smokers with subtle CT findings of centrilobular emphysema and normal findings at spirometry has increased regional heterogeneity of lung perfusion compared with never smoked subjects and smokers with normal CT image [146]. However, dynamic multi-detector CT perfusion imaging necessitates a central high-pressure bolus of contrast material and scanning a limited axial extent of the lung during a cardiac-gated scan.

Pansini et al. have demonstrated that regional alteration of lung perfusion can be assessed by dual-energy CT, matching parenchymal destruction in 47 smokers with predominant emphysema [147]. Moreover, Lee et al. have shown that the contrast-enhanced dual-energy CT can be used for the quantification of emphysema and regional perfusion evaluation by using the virtual non-contrast images and iodine map, simultaneously [148]. Assessing the distribution of pulmonary emphysema and anatomically matched parenchymal perfusion information is particularly applicable in the patient and target lobe selection for lung volume reduction surgery or bronchoscopic lung volume reduction. Data from National Emphysema Treatment Trial with more than 1000 patients undergoing lung volume reduction surgery showed that lung volume reduction surgery reduces mortality in patients with upper-lobe predominant emphysema only if there is low perfusion to the upper lobe on scintigraphy [149]. Park et al. used dual-energy CT with lung perfusion imaging for target lobe selection of bronchoscopic lung volume reduction by endobronchial valves. In that study, the target lobe was selected, if it was most hyperinflated and least perfused, and if it had no collateral ventilation with other lobes on perfusion image with dual-energy CT [150].

Ventilation Dual-Energy CT

In clinical practice, the evaluation of COPD severity is based on the result of pulmonary function test; however, pulmonary function test provides global status of lung function and does not show the regional distribution of functional abnormality. For evaluation of regional lung parenchymal ventilation, radionuclide scintigraphy or MR is used, but it is limited by its low spatial resolution. CT also can be used to depict lung ventilation with inhalation of xenon gas [151, 152]. Xenon is a radio-opaque gas and xenon gas concentration in alveolar space can be measured based on the attenuation changes on CT image (Fig. 8.22). However, because of variability in baseline lung attenuation between images due to misregistration artifacts and different respiration levels, the accurate measurement of lung ventilation function is limited, triggering great attention in the simultaneous structural and functional evaluation with single CT scanning accessible to dual-energy CT. Two stable gases, xenon and krypton, with high atomic numbers (54 for xenon and 36 for krypton) are eligible for ventilation imaging with dual-energy CT. For xenon ventilation imaging with dual-energy CT, the patient usually inhales 30% stable xenon (a mixture of 30% xenon and 70% oxygen) for 1 min to 1 min 30 s with use of a xenon gas inhalation system (Zetron V; Anzai Medical, Tokyo, Japan).

The first clinical report with xenon ventilation imaging with dual-energy CT was reported by Chae et al., investigating eight healthy volunteers and four patients with COPD. The authors have demonstrated the direct visualization of the degree of xenon gas enhancement in the lung parenchyma as a color overlay on a conventional thin-section chest CT image by material decomposition [153]. Park et al. performed two phase

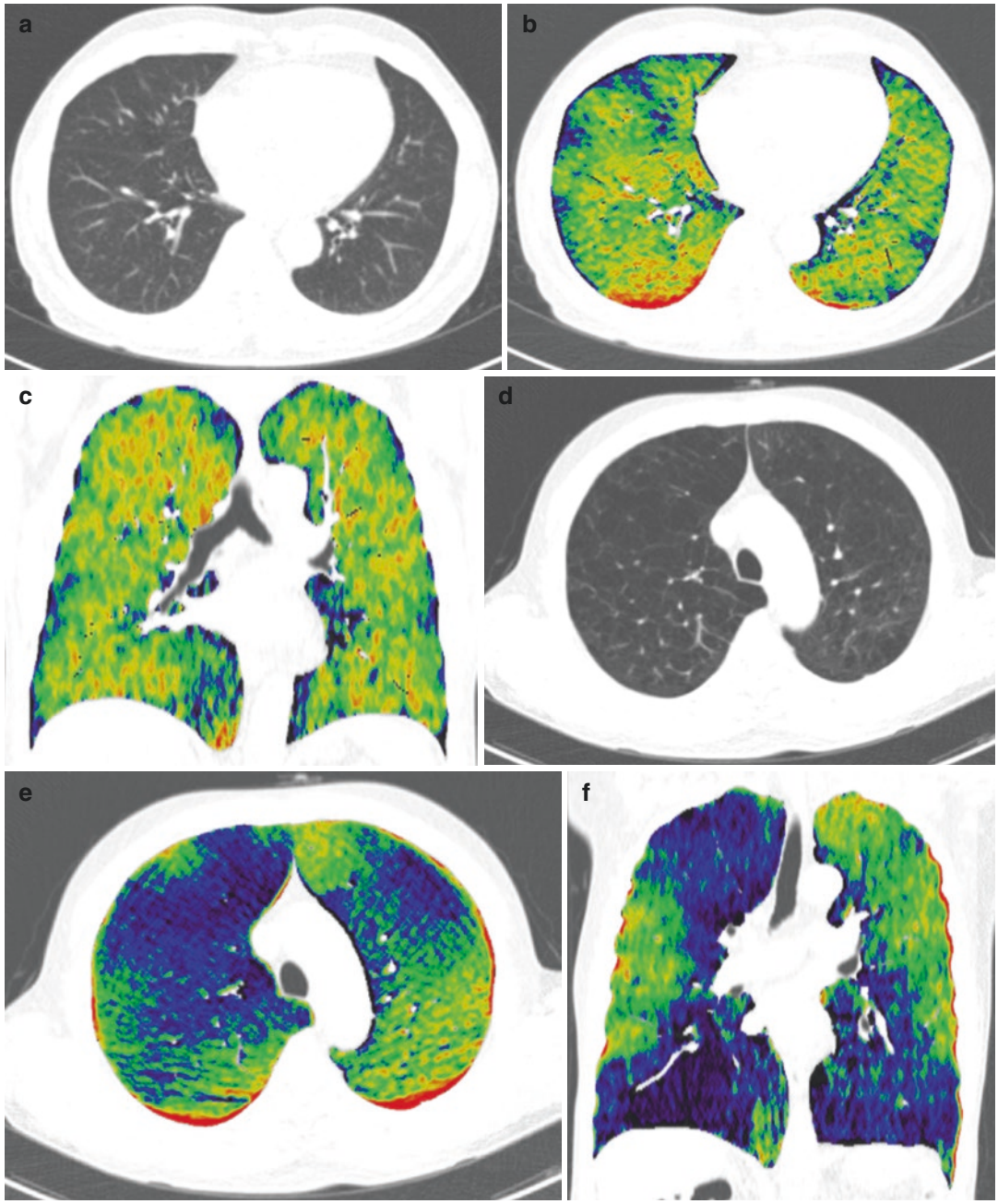

Fig. 8.22 Xenon ventilation image with dual-energy CT in COPD patient. (**a**–**c**) Dual-energy CT in COPD patient with mild emphysema. (**d**–**f**) Dual-energy CT in COPD patient with severe emphysema. (**a**, **d**) Conventional CT image and (**b**, **c**, **e**, **f**) xenon ventilation map image obtained from xenon ventilation dual-energy CT. On weighted average image (**a**, **d**), centrilobular emphysema and bronchial wall thickening in both lower lobes are noted. (**b**, **c**, **e**, **f**) In right upper lobe and left upper lobe, decreased xenon ventilation is identified, while xenon ventilation is preserved in left upper lobe posterior segment

(wash-in and wash-out phase) xenon ventilation dual-energy CT in 32 patients with COPD. And regional quantified value of xenon enhancement in abnormally low attenuating lung area on xenon-enhanced images with wash-out phase showed inverse correlation with pulmonary function test, and it showed better correlation with pulmonary function test than CT attenuation parameters [154]. Similar approaches were also reported in asthma patients. Investigating 22 asthma patients, Chae et al. have demonstrated the ventilation defects that appeared on xenon ventilation imaging with dual-energy CT in asthma patients with severe airflow limitation and airway wall thickening. And the extent of the ventilation defects on xenon-enhanced CT showed correlations with parameters of pulmonary function test [155]. Demonstration of the reversibility of airflow obstruction after inhalation of bronchodilator has been reported, and it suggested that xenon-enhanced dual-energy CT may be feasible for visualizing the changes of airflow in response to drugs in asthma patients [156–158].

Stable krypton can be an alternative to xenon for ventilation imaging with dual-energy CT due to its high atomic number, and lack of toxicity and anesthetic properties. Hachulla et al. have firstly reported the krypton ventilation imaging using dual-energy CT in COPD patients. Single CT acquisition covering the whole thorax was performed after inhalation of a mixture of 80% krypton and 20% oxygen with five respiratory maneuvers through the mask. The maximum level of krypton enhancement within the lung was 18.5 HU, which is lower than that reported with xenon, with an average maximum degree of xenon enhancement of 23.78 HU, is sufficient to detect ventilation abnormalities [159]. This single static approach in phantoms and volunteers also has been reported recently using xenon gas after a single vital capacity inhalation [160]. The single static evaluation delivers a lower radiation dose and a few or single inhalation method is more easily implementable for radiologists and patients, without side effects. However, different ventilation dynamics can be evaluated regarding the scanning method and gas inhalation method.

Combined Ventilation and Perfusion Assessment with Dual-Energy CT

Pulmonary parenchymal perfusion change or ventilation impairment was evaluated with dual-energy CT separately in COPD patients. However, the pulmonary parenchymal ventilation and perfusion are changed concurrently, and the imbalance between ventilation and perfusion is the important characteristics in the patients with COPD. Investigating ten patients with various diseases from an anesthesiological intensive care unit, Thieme et al. have reported the potential of dual-energy CT to provide both pulmonary ventilation and perfusion imaging [161]. Zhang et al. applied combined ventilation and perfusion imaging with dual-energy CT in patients with suspected pulmonary embolism [162]. Combined ventilation and perfusion imaging with dual-energy CT in patients with COPD has not yet been reported (Fig. 8.23).

Nuclear Medicine Imaging

Scintigraphy, Single-Photon Emission Computed Tomography (SPECT)

Both planar scintigraphy and SPECT image the distribution of radiotracer which is introduced into the body, and the emitted radiation from radiotracer is detected by external detectors. In contrast to scintigraphy which forms a single two-dimensional image, analogous to a planar X-ray scan, SPECT provides three-dimensional imaging about the distribution of a radiotracer by combining scintigraphic and computed tomographic technique, and allows the functional information from SPECT to be easily combined with the high-resolution anatomic information from CT. Perfusion scanning is generally performed using 99 m-technetium-labeled macroaggregated albumin (99 m Tc-MAA), which lodges in the pulmonary circulation after peripheral injection. In an animal study using pigs, perfusion SPECT has been shown to be more sensitive than HRCT to detect mild physiologic changes of elastase-induced pulmonary emphysema [163]. Moreover, Suga et al. have been demonstrated that perfusion abnormalities on breath-hold

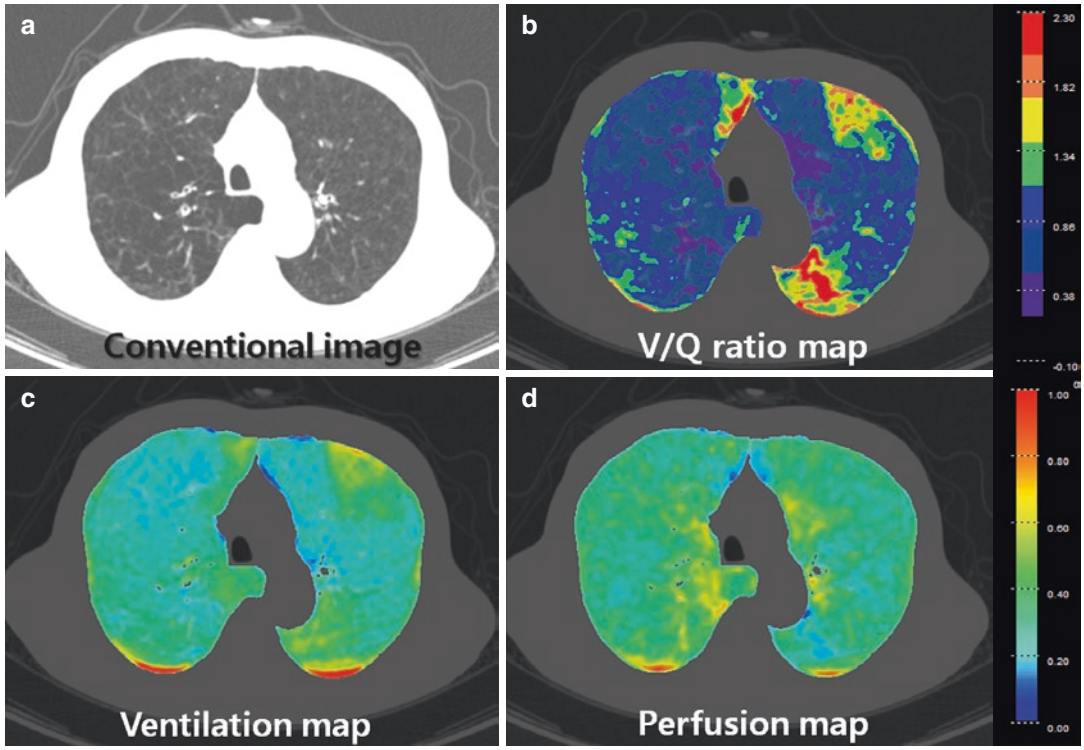

Fig. 8.23 Combined ventilation and perfusion assessment with dual-energy CT. From combined xenon ventilation and iodine perfusion CT using dual-energy CT, the conventional virtual non-contrast CT image (**a**), xenon ventilation/iodine perfusion map (**b**), ventilation map (**c**) and perfusion map (**d**) are generated. Lung parenchymal ventilation, perfusion and ventilation-perfusion imbalance with high-resolution anatomic CT information can be simultaneously evaluated with combined ventilation and perfusion dual-energy CT

SPECT-CT fusion image can better reflect the lung pathophysiology than the emphysema index on morphologic CT scan [164]. And there have been several intervention studies in COPD patients using perfusion scintigraphy and SPECT to predict and measure clinical success. As mentioned earlier, assessing the lung parenchymal perfusion has been particularly applicable in target lobe selection for lung volume reduction surgery or bronchoscopic lung volume reduction. Perfusion scintigraphy has been used in National Emphysema Treatment Trial with more than 1000 patients undergoing lung volume reduction surgery for selection of target lobe [149]. And perfusion scintigraphy was also useful for selection of target lobe for endobronchial valve therapy in advanced emphysema patients, and patients having heterogeneous emphysema with a low baseline target lobe perfusion benefited from endobronchial valve therapy [165]. Although scintigraphy and SPECT have constitutional problems, low spatial resolution and long image acquisition time, to date, they are widely applied due to their availability in many centers. Ventilation scintigraphy and SPECT use two types of inhalation radiotracers: gaseous radioisotopes or radiolabeled particulate aerosols. 81 m Kr and 133 Xe as gaseous radioisotopes have been used for ventilation scintigraphy and SPECT, and several studies with gaseous radioisotopes have demonstrated ventilation heterogeneity in COPD [166, 167]. And for radiolabeled particulate aerosol, Technegas (99 m Tc-labeled, aerosolized ultrafine carbon particle, approximately 200 nm diameter) is usually used in patients with COPD due to its small particle size [168], even in the presence of severe airflow obstruction [169]. With Technegas, the

inhomogeneities in ventilation on scintigraphy and SPECT in COPD patients have been visualized and quantified [170, 171].

Ventilation/perfusion SPECT can also be applied for the evaluation of the imbalance between ventilation and perfusion in the patients with COPD. Jogi et al. have reported significant correlation between total reduction in lung function assessed with ventilation/perfusion SPECT and spirometric lung function and emphysema severity on CT in patients with COPD [172] (Fig. 8.24). Suga et al. have described that quantitative analysis of V/Q distribution by SPECT and the standard deviation and kurtosis of the V/Q profile could be adequate indicator for the severity of lung V-Q imbalance causing gas exchange impairment in patients with emphysema [173].

Positron Emission Tomography (PET)

Regional ventilation and perfusion also can be evaluated with PET using isotope $^{13}N_2$ gas dissolved in saline solution. Brudin et al. have reported that high V/Q tended to be more common in subjects with an emphysema dominant subtype, whereas low V/Q was more common in those with a bronchial inflammation dominant subtype. Spatial heterogeneity of lung perfusion also has been described with $^{13}N_2$ saline PET, and the regional heterogeneity in perfusion has been increased in patients with mild COPD compared to healthy controls, after adjusting for regional changes in lung tissue density and ventilation. [174]. These results suggest that regional perfusion changes may precede lung parenchymal destruction in COPD. Therefore, this imaging method may serve as an early biomarker for COPD.

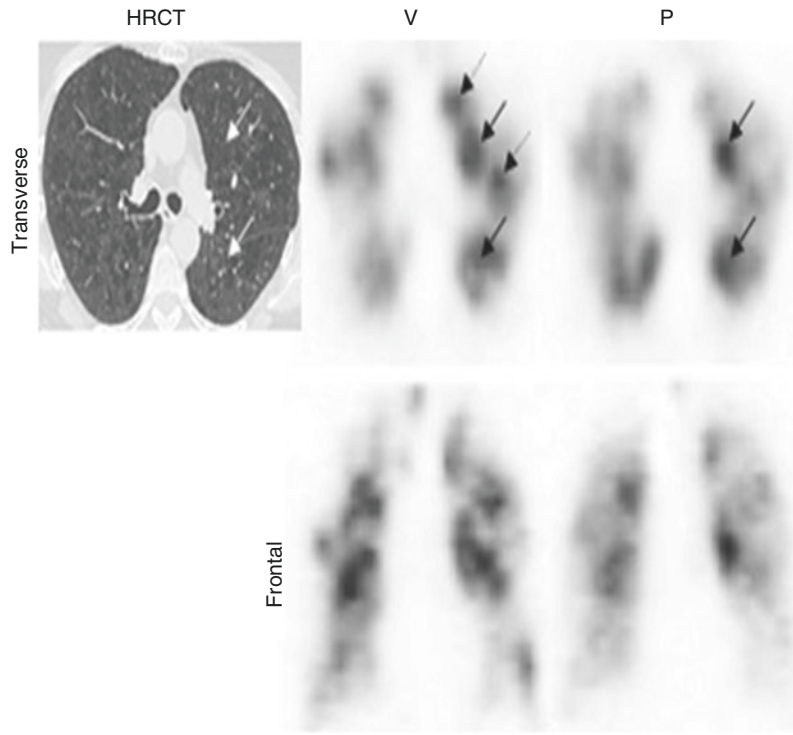

Fig. 8.24 Ventilation/perfusion SPECT. Patient with centrilobular emphysema on HRCT. Ventilation/perfusion SPECT shows uneven ventilation and perfusion. Extensive areas with reverse as well as matched ventilation/perfusion defects are found. Better perfused areas correspond to areas which are well ventilated (*black arrows*) and to better preserved parenchyma on HRCT (*white arrows*). Other areas appearing as hot spots on ventilation images are poorly perfused (*dotted arrows*). (Reprinted with permission, from reference 172)

Recent studies have been focused on systemic inflammation as a consequence of COPD, and patients with COPD are found to have higher levels of systemic biomarkers of inflammation and worse cardiovascular risk profile and prognosis [175–177]. Fluorine-18-fluorodeoxyglucose (^{18}F-FDG) is the most commonly used PET radioisotope, and it depicts increased glucose metabolism. In COPD patients, ^{18}F-FDG has been used to demonstrate both pulmonary and systemic inflammation. The pulmonary inflammation as ^{18}F-FDG uptake in COPD patients was significantly higher than in asthmatic and normal subjects [178]. Pulmonary ^{18}F-FDG uptake in usual (PiM phenotype) COPD patients was greater compared to patients with alpha-1 antitrypsin deficiency-associated emphysema (PiZ phenotype) and healthy controls, and it was correlated with FEV_1 [179]. Coulson et al. have evaluated the aortic inflammation as a measure of systemic inflammation using ^{18}F-FDG PET in seven COPD patients, five metabolic syndrome patients, and seven ex-smokers. Aortic inflammation in COPD patients was intermediate between ex-smokers and metabolic syndrome patients [180].

Optical Coherence Tomography (OCT)

OCT is an imaging method utilizing the refraction of light waves as it passes through tissues, and measures the lung structure with endobronchial approach. A fiberoptic probe with a near-infrared optical probe is introduced into the airways via a bronchoscope and the reflected light by the tissue is detected and reconstructed into an image. The spatial resolution of OCT is much higher than CT with the ability to resolve structures up to micrometers and distinguish between different tissue types within the airways. Thus, the main strength of OCT in COPD is the ability assessing small airway morphology in vivo. Coxson et al. have demonstrated an excellent correlation between airway lumen and wall area measured by OCT and by CT [181]. Furthermore, OCT airway dimensions measured at the fifth generation bronchi showed a stronger negative correlation with the subject's FEV_1 than CT, and had greater sensitivity in detecting changes in wall measurement than CT measurements. And OCT also provided data on airway wall morphology and subepithelial remodeling and collagen deposition. While OCT is not widely applicable to date, the novel ability on directly assessing small airway disease in COPD patients may allow increasing utilization of OCT in research and clinical practice.

References

1. Larke FJ, Kruger RL, Cagnon CH, Flynn MJ, McNitt-Gray MM, Wu X, et al. Estimated radiation dose associated with low-dose chest CT of average-size participants in the National Lung Screening Trial. AJR Am J Roentgenol. 2011;197(5):1165–9. doi:10.2214/AJR.11.6533.
2. Newell JD Jr, Sieren J, Hoffman EA. Development of quantitative computed tomography lung protocols. J Thorac Imaging. 2013;28(5):266–71. doi:10.1097/RTI.0b013e31829f6796.
3. Mayo JR. CT evaluation of diffuse infiltrative lung disease: dose considerations and optimal technique. J Thorac Imaging. 2009;24(4):252–9. doi:10.1097/RTI.0b013e3181c227b2.
4. Madani A, De Maertelaer V, Zanen J, Gevenois PA. Pulmonary emphysema: radiation dose and section thickness at multidetector CT quantification—comparison with macroscopic and microscopic morphometry. Radiology. 2007;243(1):250–7. doi:10.1148/radiol.2431060194.
5. Kemerink GJ, Kruize HH, Lamers RJ, van Engelshoven JM. CT lung densitometry: dependence of CT number histograms on sample volume and consequences for scan protocol comparability. J Comput Assist Tomogr. 1997;21(6):948–54.
6. Boedeker KL, McNitt-Gray MF, Rogers SR, Truong DA, Brown MS, Gjertson DW, et al. Emphysema: effect of reconstruction algorithm on CT imaging measures. Radiology. 2004;232(1):295–301. doi:10.1148/radiol.2321030383.
7. Choo JY, Goo JM, Lee CH, Park CM, Park SJ, Shim MS. Quantitative analysis of emphysema and airway measurements according to iterative reconstruction algorithms: comparison of filtered back projection, adaptive statistical iterative reconstruction and model-based iterative reconstruction. Eur Radiol. 2014;24(4):799–806. doi:10.1007/s00330-013-3078-5.
8. Mets OM, Willemink MJ, de Kort FP, Mol CP, Leiner T, Oudkerk M, et al. The effect of iterative reconstruction on computed tomography assessment of emphysema, air trapping and airway dimensions.

Eur Radiol. 2012;22(10):2103–9. doi:10.1007/s00330-012-2489-z.
9. Nishio M, Matsumoto S, Ohno Y, Sugihara N, Inokawa H, Yoshikawa T, et al. Emphysema quantification by low-dose CT: potential impact of adaptive iterative dose reduction using 3D processing. AJR Am J Roentgenol. 2012;199(3):595–601. doi:10.2214/AJR.11.8174.
10. Schroeder JD, McKenzie AS, Zach JA, Wilson CG, Curran-Everett D, Stinson DS, et al. Relationships between airflow obstruction and quantitative CT measurements of emphysema, air trapping, and airways in subjects with and without chronic obstructive pulmonary disease. AJR Am J Roentgenol. 2013;201(3):W460–70. doi:10.2214/AJR.12.10102.
11. Stockley RA, Mannino D, Barnes PJ. Burden and pathogenesis of chronic obstructive pulmonary disease. Proc Am Thorac Soc. 2009;6(6):524–6. doi:10.1513/pats.200904-016DS.
12. Roy K, Smith J, Kolsum U, Borrill Z, Vestbo J, Singh D. COPD phenotype description using principal components analysis. Respir Res. 2009;10:41. doi:10.1186/1465-9921-10-41.
13. Bergin C, Muller N, Nichols DM, Lillington G, Hogg JC, Mullen B, et al. The diagnosis of emphysema. A computed tomographic-pathologic correlation. Am Rev Respir Dis. 1986;133(4):541–6.
14. Bafadhel M, Umar I, Gupta S, Raj JV, Vara DD, Entwisle JJ, et al. The role of CT scanning in multidimensional phenotyping of COPD. Chest. 2011;140(3):634–42. doi:10.1378/chest.10-3007.
15. O'Brien C, Guest PJ, Hill SL, Stockley RA. Physiological and radiological characterisation of patients diagnosed with chronic obstructive pulmonary disease in primary care. Thorax. 2000;55(8):635–42.
16. McDonough JE, Yuan R, Suzuki M, Seyednejad N, Elliott WM, Sanchez PG, et al. Small-airway obstruction and emphysema in chronic obstructive pulmonary disease. N Engl J Med. 2011;365(17):1567–75. doi:10.1056/NEJMoa1106955.
17. Lehouck A, Boonen S, Decramer M, Janssens W. COPD, bone metabolism, and osteoporosis. Chest. 2011;139(3):648–57. doi:10.1378/chest.10-1427.
18. Miller RR, Muller NL, Vedal S, Morrison NJ, Staples CA. Limitations of computed tomography in the assessment of emphysema. Am Rev Respir Dis. 1989;139(4):980–3. doi:10.1164/ajrccm/139.4.980.
19. Kim SS, Seo JB, Lee HY, Nevrekar DV, Forssen AV, Crapo JD, et al. Chronic obstructive pulmonary disease: lobe-based visual assessment of volumetric CT by using standard images—comparison with quantitative CT and pulmonary function test in the COPDGene study. Radiology. 2013;266(2):626–35. doi:10.1148/radiol.12120385.
20. Cavigli E, Camiciottoli G, Diciotti S, Orlandi I, Spinelli C, Meoni E, et al. Whole-lung densitometry versus visual assessment of emphysema. Eur Radiol. 2009;19(7):1686–92. doi:10.1007/s00330-009-1320-y.
21. Bankier AA, De Maertelaer V, Keyzer C, Gevenois PA. Pulmonary emphysema: subjective visual grading versus objective quantification with macroscopic morphometry and thin-section CT densitometry. Radiology. 1999;211(3):851–8. doi:10.1148/radiology.211.3.r99jn05851.
22. Group COCW, Barr RG, Berkowitz EA, Bigazzi F, Bode F, Bon J, et al. A combined pulmonary-radiology workshop for visual evaluation of COPD: study design, chest CT findings and concordance with quantitative evaluation. COPD. 2012;9(2):151–9. doi:10.3109/15412555.2012.654923.
23. Hayhurst MD, MacNee W, Flenley DC, Wright D, McLean A, Lamb D, et al. Diagnosis of pulmonary emphysema by computerised tomography. Lancet. 1984;2(8398):320–2.
24. Muller NL, Staples CA, Miller RR, Abboud RT. "Density mask". An objective method to quantitate emphysema using computed tomography. Chest. 1988;94(4):782–7.
25. Madani A, Zanen J, de Maertelaer V, Gevenois PA. Pulmonary emphysema: objective quantification at multi-detector row CT—comparison with macroscopic and microscopic morphometry. Radiology. 2006;238(3):1036–43. doi:10.1148/radiol.2382042196.
26. Dirksen A, Friis M, Olesen KP, Skovgaard LT, Sorensen K. Progress of emphysema in severe alpha 1-antitrypsin deficiency as assessed by annual CT. Acta Radiol. 1997;38(5):826–32.
27. Dirksen A. Monitoring the progress of emphysema by repeat computed tomography scans with focus on noise reduction. Proc Am Thorac Soc. 2008;5(9):925–8. doi:10.1513/pats.200804-033QC.
28. Heussel CP, Herth FJ, Kappes J, Hantusch R, Hartlieb S, Weinheimer O, et al. Fully automatic quantitative assessment of emphysema in computed tomography: comparison with pulmonary function testing and normal values. Eur Radiol. 2009;19(10):2391–402. doi:10.1007/s00330-009-1437-z.
29. Stolk J, Dirksen A, van der Lugt AA, Hutsebaut J, Mathieu J, de Ree J, et al. Repeatability of lung density measurements with low-dose computed tomography in subjects with alpha-1-antitrypsin deficiency-associated emphysema. Investig Radiol. 2001;36(11):648–51.
30. Gietema HA, Muller NL, Fauerbach PV, Sharma S, Edwards LD, Camp PG, et al. Quantifying the extent of emphysema: factors associated with radiologists' estimations and quantitative indices of emphysema severity using the ECLIPSE cohort. Acad Radiol. 2011;18(6):661–71. doi:10.1016/j.acra.2011.01.011.
31. Parr DG, Stoel BC, Stolk J, Stockley RA. Pattern of emphysema distribution in alpha1-antitrypsin deficiency influences lung function impairment.

Am J Respir Crit Care Med. 2004;170(11):1172–8. doi:10.1164/rccm.200406-761OC.
32. Nakano Y, Sakai H, Muro S, Hirai T, Oku Y, Nishimura K, et al. Comparison of low attenuation areas on computed tomographic scans between inner and outer segments of the lung in patients with chronic obstructive pulmonary disease: incidence and contribution to lung function. Thorax. 1999;54(5):384–9.
33. Chae EJ, Seo JB, Song JW, Kim N, Park BW, Lee YK, et al. Slope of emphysema index: an objective descriptor of regional heterogeneity of emphysema and an independent determinant of pulmonary function. AJR Am J Roentgenol. 2010;194(3):W248–55. doi:10.2214/AJR.09.2672.
34. Nakano Y, Coxson HO, Bosan S, Rogers RM, Sciurba FC, Keenan RJ, et al. Core to rind distribution of severe emphysema predicts outcome of lung volume reduction surgery. Am J Respir Crit Care Med. 2001;164(12):2195–9. doi:10.1164/ajrccm.164.12.2012140.
35. Martinez-Garcia MA, Soler-Cataluna JJ, Donat Sanz Y, Catalan Serra P, Agramunt Lerma M, Ballestin Vicente J, et al. Factors associated with bronchiectasis in patients with COPD. Chest. 2011;140(5):1130–7. doi:10.1378/chest.10-1758.
36. Grydeland TB, Thorsen E, Dirksen A, Jensen R, Coxson HO, Pillai SG, et al. Quantitative CT measures of emphysema and airway wall thickness are related to D(L)CO. Respir Med. 2011;105(3):343–51. doi:10.1016/j.rmed.2010.10.018.
37. Nakano Y, Muro S, Sakai H, Hirai T, Chin K, Tsukino M, et al. Computed tomographic measurements of airway dimensions and emphysema in smokers. Correlation with lung function. Am J Respir Crit Care Med. 2000;162(3 Pt 1):1102–8. doi:10.1164/ajrccm.162.3.9907120.
38. Washko GR, Dransfield MT, Estepar RS, Diaz A, Matsuoka S, Yamashiro T, et al. Airway wall attenuation: a biomarker of airway disease in subjects with COPD. J Appl Physiol. 2009;107(1):185–91. doi:10.1152/japplphysiol.00216.2009.
39. Nakano Y, Wong JC, de Jong PA, Buzatu L, Nagao T, Coxson HO, et al. The prediction of small airway dimensions using computed tomography. Am J Respir Crit Care Med. 2005;171(2):142–6. doi:10.1164/rccm.200407-874OC.
40. Achenbach T, Weinheimer O, Biedermann A, Schmitt S, Freudenstein D, Goutham E, et al. MDCT assessment of airway wall thickness in COPD patients using a new method: correlations with pulmonary function tests. Eur Radiol. 2008;18(12):2731–8. doi:10.1007/s00330-008-1089-4.
41. Han MK, Kazerooni EA, Lynch DA, Liu LX, Murray S, Curtis JL, et al. Chronic obstructive pulmonary disease exacerbations in the COPDGene study: associated radiologic phenotypes. Radiology. 2011;261(1):274–82. doi:10.1148/radiol.11110173.
42. Lee HJ, Seo JB, Chae EJ, Kim N, Lee CW, Oh YM, et al. Tracheal morphology and collapse in COPD: correlation with CT indices and pulmonary function test. Eur J Radiol. 2011;80(3):e531–5. doi:10.1016/j.ejrad.2010.12.062.
43. Boiselle PM, Litmanovich DE, Michaud G, Roberts DH, Loring SH, Womble HM, et al. Dynamic expiratory tracheal collapse in morbidly obese COPD patients. COPD. 2013;10(5):604–10. doi:10.3109/15412555.2013.781149.
44. Regan EA, Hokanson JE, Murphy JR, Make B, Lynch DA, Beaty TH, et al. Genetic epidemiology of COPD (COPDGene) study design. COPD. 2010;7(1):32–43. doi:10.3109/15412550903499522.
45. Matsuoka S, Kurihara Y, Yagihashi K, Nakajima Y. Quantitative assessment of peripheral airway obstruction on paired expiratory/inspiratory thin-section computed tomography in chronic obstructive pulmonary disease with emphysema. J Comput Assist Tomogr. 2007;31(3):384–9. doi:10.1097/01.rct.0000243457.00437.10.
46. Matsuoka S, Kurihara Y, Yagihashi K, Hoshino M, Watanabe N, Nakajima Y. Quantitative assessment of air trapping in chronic obstructive pulmonary disease using inspiratory and expiratory volumetric MDCT. AJR Am J Roentgenol. 2008;190(3):762–9. doi:10.2214/AJR.07.2820.
47. Yamashiro T, Matsuoka S, Bartholmai BJ, San Jose Estepar R, Ross JC, Diaz A, et al. Collapsibility of lung volume by paired inspiratory and expiratory CT scans: correlations with lung function and mean lung density. Acad Radiol. 2010;17(4):489–95. doi:10.1016/j.acra.2009.11.004.
48. Lee YK, Oh YM, Lee JH, Kim EK, Lee JH, Kim N, et al. Quantitative assessment of emphysema, air trapping, and airway thickening on computed tomography. Lung. 2008;186(3):157–65. doi:10.1007/s00408-008-9071-0.
49. Galban CJ, Han MK, Boes JL, Chughtai KA, Meyer CR, Johnson TD, et al. Computed tomography-based biomarker provides unique signature for diagnosis of COPD phenotypes and disease progression. Nat Med. 2012;18(11):1711–5. doi:10.1038/nm.2971.
50. Barbosa EM Jr, Song G, Tustison N, Kreider M, Gee JC, Gefter WB, et al. Computational analysis of thoracic multidetector row HRCT for segmentation and quantification of small airway air trapping and emphysema in obstructive pulmonary disease. Acad Radiol. 2011;18(10):1258–69. doi:10.1016/j.acra.2011.06.004.
51. Ginsburg SB, Lynch DA, Bowler RP, Schroeder JD. Automated texture-based quantification of centrilobular nodularity and centrilobular emphysema in chest CT images. Acad Radiol. 2012;19(10):1241–51. doi:10.1016/j.acra.2012.04.020.
52. Park YS, Seo JB, Kim N, Chae EJ, Oh YM, Lee SD, et al. Texture-based quantification of pulmonary emphysema on high-resolution computed tomography: comparison with density-based quantification and correlation with pulmonary function test.

Investig Radiol. 2008;43(6):395–402. doi:10.1097/RLI.0b013e31816901c7.
53. Barr RG, Mesia-Vela S, Austin JH, Basner RC, Keller BM, Reeves AP, et al. Impaired flow-mediated dilation is associated with low pulmonary function and emphysema in ex-smokers: the emphysema and cancer action project (EMCAP) study. Am J Respir Crit Care Med. 2007;176(12):1200–7. doi:10.1164/rccm.200707-980OC.
54. Ross JC, Estepar RS, Diaz A, Westin CF, Kikinis R, Silverman EK, et al. Lung extraction, lobe segmentation and hierarchical region assessment for quantitative analysis on high resolution computed tomography images. Med Image Comput Comput Assist Interv. 2009;12(Pt 2):690–8.
55. Xiao C, Staring M, Shamonin D, Reiber JH, Stolk J, Stoel BC. A strain energy filter for 3D vessel enhancement with application to pulmonary CT images. Med Image Anal. 2011;15(1):112–24. doi:10.1016/j.media.2010.08.003.
56. Matsuoka S, Washko GR, Dransfield MT, Yamashiro T, San Jose Estepar R, Diaz A, et al. Quantitative CT measurement of cross-sectional area of small pulmonary vessel in COPD: correlations with emphysema and airflow limitation. Acad Radiol. 2010;17(1):93–9. doi:10.1016/j.acra.2009.07.022.
57. Harrison RA, Siminoski K, Vethanayagam D, Majumdar SR. Osteoporosis-related kyphosis and impairments in pulmonary function: a systematic review. J Bone Miner Res Off J Am Soc Bone Miner Res. 2007;22(3):447–57. doi:10.1359/jbmr.061202.
58. Ohara T, Hirai T, Muro S, Haruna A, Terada K, Kinose D, et al. Relationship between pulmonary emphysema and osteoporosis assessed by CT in patients with COPD. Chest. 2008;134(6):1244–9. doi:10.1378/chest.07-3054.
59. Kiyokawa H, Muro S, Oguma T, Sato S, Tanabe N, Takahashi T, et al. Impact of COPD exacerbations on osteoporosis assessed by chest CT scan. COPD. 2012;9(3):235–42. doi:10.3109/15412555.2011.650243.
60. Marquis K, Debigare R, Lacasse Y, LeBlanc P, Jobin J, Carrier G, et al. Midthigh muscle cross-sectional area is a better predictor of mortality than body mass index in patients with chronic obstructive pulmonary disease. Am J Respir Crit Care Med. 2002;166(6):809–13. doi:10.1164/rccm.2107031.
61. Soler-Cataluna JJ, Sanchez-Sanchez L, Martinez-Garcia MA, Sanchez PR, Salcedo E, Navarro M. Mid-arm muscle area is a better predictor of mortality than body mass index in COPD. Chest. 2005;128(4):2108–15. doi:10.1378/chest.128.4.2108.
62. Park MJ, Cho JM, Jeon KN, Bae KS, Kim HC, Choi DS, et al. Mass and fat infiltration of intercostal muscles measured by CT histogram analysis and their correlations with COPD severity. Acad Radiol. 2014;21(6):711–7. doi:10.1016/j.acra.2014.02.003.
63. Sin DD, Wu L, Man SF. The relationship between reduced lung function and cardiovascular mortality: a population-based study and a systematic review of the literature. Chest. 2005;127(6):1952–9. doi:10.1378/chest.127.6.1952.
64. Sin DD, Man SF. Chronic obstructive pulmonary disease as a risk factor for cardiovascular morbidity and mortality. Proc Am Thorac Soc. 2005;2(1):8–11. doi:10.1513/pats.200404-032MS.
65. Chae EJ, Seo JB, Oh YM, Lee JS, Jung Y, Lee SD. Severity of systemic calcified atherosclerosis is associated with airflow limitation and emphysema. J Comput Assist Tomogr. 2013;37(5):743–9. doi:10.1097/RCT.0b013e318299f9e7.
66. Ayres SM, Griesbach SJ, Reimold F, Evans RG. Bronchial component in chronic obstructive lung disease. Am J Med. 1974;57(2):183–91.
67. Pare PD, Lawson LM, Brooks LA. Patterns of response to inhaled bronchodilators in asthmatics. Am Rev Respir Dis. 1983;127(6):680–5.
68. Lee JS, Huh JW, Chae EJ, Seo JB, Ra SW, Lee JH, et al. Response patterns to bronchodilator and quantitative computed tomography in chronic obstructive pulmonary disease. Clin Physiol Funct Imaging. 2012;32(1):12–8. doi:10.1111/j.1475-097X.2011.01046.x.
69. Dirksen A, Piitulainen E, Parr DG, Deng C, Wencker M, Shaker SB, et al. Exploring the role of CT densitometry: a randomised study of augmentation therapy in alpha1-antitrypsin deficiency. Eur Respir J. 2009;33(6):1345–53. doi:10.1183/09031936.00159408.
70. Kim SS, Seo JB, Kim N, Chae EJ, Lee YK, Oh YM, et al. Improved correlation between CT emphysema quantification and pulmonary function test by density correction of volumetric CT data based on air and aortic density. Eur J Radiol. 2014;83(1):57–63. doi:10.1016/j.ejrad.2012.02.021.
71. Parr DG, Stoel BC, Stolk J, Nightingale PG, Stockley RA. Influence of calibration on densitometric studies of emphysema progression using computed tomography. Am J Respir Crit Care Med. 2004;170(8):883–90. doi:10.1164/rccm.200403-326OC.
72. Madani A, Van Muylem A, Gevenois PA. Pulmonary emphysema: effect of lung volume on objective quantification at thin-section CT. Radiology. 2010;257(1):260–8. doi:10.1148/radiol.10091446.
73. Grydeland TB, Dirksen A, Coxson HO, Pillai SG, Sharma S, Eide GE, et al. Quantitative computed tomography: emphysema and airway wall thickness by sex, age and smoking. Eur Respir J. 2009;34(4):858–65. doi:10.1183/09031936.00167908.
74. Camiciottoli G, Cavigli E, Grassi L, Diciotti S, Orlandi I, Zappa M, et al. Prevalence and correlates of pulmonary emphysema in smokers and former smokers. A densitometric study of participants in the ITALUNG trial. Eur Radiol. 2009;19(1):58–66. doi:10.1007/s00330-008-1131-6.
75. Ley-Zaporozhan J, Ley S, Kauczor HU. Morphological and functional imaging in COPD with CT and MRI: present and future. Eur Radiol. 2008;18(3):510–21. doi:10.1007/s00330-007-0772-1.

76. Bankier AA, O'Donnell CR, Mai VM, Storey P, De Maertelaer V, Edelman RR, et al. Impact of lung volume on MR signal intensity changes of the lung parenchyma. J Magn Reson Imaging. 2004;20(6):961–6. doi:10.1002/jmri.20198.
77. Rajaram S, Swift AJ, Capener D, Telfer A, Davies C, Hill C, et al. Lung morphology assessment with balanced steady-state free precession MR imaging compared with CT. Radiology. 2012;263(2):569–77. doi:10.1148/radiol.12110990.
78. Ley-Zaporozhan J, Ley S, Eberhardt R, Kauczor HU, Heussel CP. Visualization of morphological parenchymal changes in emphysema: comparison of different MRI sequences to 3D-HRCT. Eur J Radiol. 2010;73(1):43–9. doi:10.1016/j.ejrad.2008.09.029.
79. Ley-Zaporozhan J, Ley S, Kauczor HU. Proton MRI in COPD. COPD. 2007;4(1):55–65. doi:10.1080/15412550701198719.
80. Vogel-Claussen J, Renne J, Hinrichs J, Schonfeld C, Gutberlet M, Schaumann F, et al. Quantification of pulmonary inflammation after segmental allergen challenge using turbo-inversion recovery-magnitude magnetic resonance imaging. Am J Respir Crit Care Med. 2014;189(6):650–7. doi:10.1164/rccm.201310-1825OC.
81. Iwasawa T, Takahashi H, Ogura T, Asakura A, Gotoh T, Kagei S, et al. Correlation of lung parenchymal MR signal intensity with pulmonary function tests and quantitative computed tomography (CT) evaluation: a pilot study. J Magn Reson Imaging. 2007;26(6):1530–6. doi:10.1002/jmri.21183.
82. Mayo JR, MacKay A, Muller NL. MR imaging of the lungs: value of short TE spin-echo pulse sequences. AJR Am J Roentgenol. 1992;159(5):951–6. doi:10.2214/ajr.159.5.1414805.
83. Bergin CJ, Pauly JM, Macovski A. Lung parenchyma: projection reconstruction MR imaging. Radiology. 1991;179(3):777–81. doi:10.1148/radiology.179.3.2027991.
84. Ohno Y, Koyama H, Yoshikawa T, Matsumoto K, Takahashi M, Van Cauteren M, et al. T2* measurements of 3-T MRI with ultrashort TEs: capabilities of pulmonary function assessment and clinical stage classification in smokers. AJR Am J Roentgenol. 2011;197(2):W279–85. doi:10.2214/AJR.10.5350.
85. Takahashi M, Togao O, Obara M, van Cauteren M, Ohno Y, Doi S, et al. Ultra-short echo time (UTE) MR imaging of the lung: comparison between normal and emphysematous lungs in mutant mice. J Magn Reson Imaging. 2010;32(2):326–33. doi:10.1002/jmri.22267.
86. Johnson KM, Fain SB, Schiebler ML, Nagle S. Optimized 3D ultrashort echo time pulmonary MRI. Magn Reson Med. 2013;70(5):1241–50. doi:10.1002/mrm.24570.
87. Bianchi A, Ozier A, Ousova O, Raffard G, Cremillieux Y. Ultrashort-TE MRI longitudinal study and characterization of a chronic model of asthma in mice: inflammation and bronchial remodeling assessment. NMR Biomed. 2013;26(11):1451–9. doi:10.1002/nbm.2975.
88. Puderbach M, Eichinger M, Gahr J, Ley S, Tuengerthal S, Schmahl A, et al. Proton MRI appearance of cystic fibrosis: comparison to CT. Eur Radiol. 2007;17(3):716–24. doi:10.1007/s00330-006-0373-4.
89. Biederer J, Both M, Graessner J, Liess C, Jakob P, Reuter M, et al. Lung morphology: fast MR imaging assessment with a volumetric interpolated breath-hold technique: initial experience with patients. Radiology. 2003;226(1):242–9. doi:10.1148/radiol.2261011974.
90. Beckmann N, Cannet C, Zurbruegg S, Rudin M, Tigani B. Proton MRI of lung parenchyma reflects allergen-induced airway remodeling and endotoxin-aroused hyporesponsiveness: a step toward ventilation studies in spontaneously breathing rats. Magn Reson Med. 2004;52(2):258–68. doi:10.1002/mrm.20127.
91. Ogasawara N, Suga K, Zaki M, Okada M, Kawakami Y, Matsunaga N. Assessment of lung perfusion impairment in patients with pulmonary artery-occlusive and chronic obstructive pulmonary diseases with noncontrast electrocardiogram-gated fast-spin-echo perfusion MR imaging. J Magn Reson Imaging. 2004;20(4):601–11. doi:10.1002/jmri.20150.
92. Suga K, Ogasawara N, Okada M, Hara A, Matsunaga N. Potential of noncontrast electrocardiogram-gated half-fourier fast-spin-echo magnetic resonance imaging to monitor dynamically altered perfusion in regional lung. Investig Radiol. 2002;37(11):615–25. doi:10.1097/01.RLI.0000031079.78361.7D.
93. Hatabu H, Tadamura E, Levin DL, Chen Q, Li W, Kim D, et al. Quantitative assessment of pulmonary perfusion with dynamic contrast-enhanced MRI. Magn Reson Med. 1999;42(6):1033–8.
94. Levin DL, Chen Q, Zhang M, Edelman RR, Hatabu H. Evaluation of regional pulmonary perfusion using ultrafast magnetic resonance imaging. Magn Reson Med. 2001;46(1):166–71.
95. Keilholz SD, Mai VM, Berr SS, Fujiwara N, Hagspiel KD. Comparison of first-pass Gd-DOTA and FAIRER MR perfusion imaging in a rabbit model of pulmonary embolism. J Magn Reson Imaging. 2002;16(2):168–71. doi:10.1002/jmri.10138.
96. Korosec FR, Frayne R, Grist TM, Mistretta CA. Time-resolved contrast-enhanced 3D MR angiography. Magn Reson Med. 1996;36(3):345–51.
97. Fink C, Ley S, Kroeker R, Requardt M, Kauczor HU, Bock M. Time-resolved contrast-enhanced three-dimensional magnetic resonance angiography of the chest: combination of parallel imaging with view sharing (TREAT). Investig Radiol. 2005;40(1):40–8.
98. Fink C, Ley S, Risse F, Eichinger M, Zaporozhan J, Buhmann R, et al. Effect of inspiratory and expiratory breathhold on pulmonary perfusion: assessment by pulmonary perfusion magnetic resonance imaging. Investig Radiol. 2005;40(2):72–9.

99. Dehnert C, Risse F, Ley S, Kuder TA, Buhmann R, Puderbach M, et al. Magnetic resonance imaging of uneven pulmonary perfusion in hypoxia in humans. Am J Respir Crit Care Med. 2006;174(10):1132–8. doi:10.1164/rccm.200606-780OC.
100. Sergiacomi G, Sodani G, Fabiano S, Manenti G, Spinelli A, Konda D, et al. MRI lung perfusion 2D dynamic breath-hold technique in patients with severe emphysema. In Vivo. 2003;17(4):319–24.
101. Molinari F, Fink C, Risse F, Tuengerthal S, Bonomo L, Kauczor HU. Assessment of differential pulmonary blood flow using perfusion magnetic resonance imaging: comparison with radionuclide perfusion scintigraphy. Investig Radiol. 2006;41(8):624–30. doi:10.1097/01.rli.0000225399.65609.45.
102. Morino S, Toba T, Araki M, Azuma T, Tsutsumi S, Tao H, et al. Noninvasive assessment of pulmonary emphysema using dynamic contrast-enhanced magnetic resonance imaging. Exp Lung Res. 2006;32(1–2):55–67. doi:10.1080/01902140600691548.
103. Ley-Zaporozhan J, Ley S, Eberhardt R, Weinheimer O, Fink C, Puderbach M, et al. Assessment of the relationship between lung parenchymal destruction and impaired pulmonary perfusion on a lobar level in patients with emphysema. Eur J Radiol. 2007;63(1):76–83. doi:10.1016/j.ejrad.2007.01.020.
104. Jang YM, Oh YM, Seo JB, Kim N, Chae EJ, Lee YK, et al. Quantitatively assessed dynamic contrast-enhanced magnetic resonance imaging in patients with chronic obstructive pulmonary disease: correlation of perfusion parameters with pulmonary function test and quantitative computed tomography. Investig Radiol. 2008;43(6):403–10. doi:10.1097/RLI.0b013e31816901ab.
105. Ohno Y, Hatabu H, Murase K, Higashino T, Kawamitsu H, Watanabe H, et al. Quantitative assessment of regional pulmonary perfusion in the entire lung using three-dimensional ultrafast dynamic contrast-enhanced magnetic resonance imaging: preliminary experience in 40 subjects. J Magn Reson Imaging. 2004;20(3):353–65. doi:10.1002/jmri.20137.
106. Tadamura E, Hatabu H, Li W, Prasad PV, Edelman RR. Effect of oxygen inhalation on relaxation times in various tissues. J Magn Reson Imaging. 1997;7(1):220–5.
107. Brooks RA, Di Chiro G. Magnetic resonance imaging of stationary blood: a review. Med Phys. 1987;14(6):903–13.
108. Thulborn KR, Waterton JC, Matthews PM, Radda GK. Oxygenation dependence of the transverse relaxation time of water protons in whole blood at high field. Biochim Biophys Acta. 1982;714(2):265–70.
109. Ohno Y, Chen Q, Hatabu H. Oxygen-enhanced magnetic resonance ventilation imaging of lung. Eur J Radiol. 2001;37(3):164–71.
110. Bauman G, Eichinger M. Ventilation and perfusion magnetic resonance imaging of the lung. Pol J Radiol. 2012;77(1):37–46.
111. Ohno Y, Hatabu H. Basics concepts and clinical applications of oxygen-enhanced MR imaging. Eur J Radiol. 2007;64(3):320–8. doi:10.1016/j.ejrad.2007.08.006.
112. Ohno Y, Hatabu H, Takenaka D, Van Cauteren M, Fujii M, Sugimura K. Dynamic oxygen-enhanced MRI reflects diffusing capacity of the lung. Magn Reson Med. 2002;47(6):1139–44. doi:10.1002/mrm.10168.
113. Ohno Y, Hatabu H, Takenaka D, Adachi S, Van Cauteren M, Sugimura K. Oxygen-enhanced MR ventilation imaging of the lung: preliminary clinical experience in 25 subjects. AJR Am J Roentgenol. 2001;177(1):185–94. doi:10.2214/ajr.177.1.1770185.
114. Kirby M, Mathew L, Wheatley A, Santyr GE, McCormack DG, Parraga G. Chronic obstructive pulmonary disease: longitudinal hyperpolarized (3) He MR imaging. Radiology. 2010;256(1):280–9. doi:10.1148/radiol.10091937.
115. Kaushik SS, Cleveland ZI, Cofer GP, Metz G, Beaver D, Nouls J, et al. Diffusion-weighted hyperpolarized 129Xe MRI in healthy volunteers and subjects with chronic obstructive pulmonary disease. Magn Reson Med. 2011;65(4):1154–65. doi:10.1002/mrm.22697.
116. Altes TA, Salerno M. Hyperpolarized gas MR imaging of the lung. J Thorac Imaging. 2004;19(4):250–8.
117. de Lange EE, Altes TA, Patrie JT, Gaare JD, Knake JJ, Mugler JP III, et al. Evaluation of asthma with hyperpolarized helium-3 MRI: correlation with clinical severity and spirometry. Chest. 2006;130(4):1055–62. doi:10.1378/chest.130.4.1055.
118. van Beek EJ, Wild JM, Kauczor HU, Schreiber W, Mugler JP III, de Lange EE. Functional MRI of the lung using hyperpolarized 3-helium gas. J Magn Reson Imaging. 2004;20(4):540–54. doi:10.1002/jmri.20154.
119. Frahm J, Haase A, Matthaei D. Rapid NMR imaging of dynamic processes using the FLASH technique. Magn Reson Med. 1986;3(2):321–7.
120. Bock M. Simultaneous T2* and diffusion measurements with 3He. Magn Reson Med. 1997;38(6):890–5.
121. Salerno M, Altes TA, Brookeman JR, de Lange EE, Mugler JP III. Dynamic spiral MRI of pulmonary gas flow using hyperpolarized (3)He: preliminary studies in healthy and diseased lungs. Magn Reson Med. 2001;46(4):667–77.
122. Deninger AJ, Eberle B, Ebert M, Grossmann T, Heil W, Kauczor H, et al. Quantification of regional intrapulmonary oxygen partial pressure evolution during apnea by (3)He MRI. J Magn Reson. 1999;141(2):207–16. doi:10.1006/jmre.1999.1902.
123. Deninger AJ, Eberle B, Bermuth J, Escat B, Markstaller K, Schmiedeskamp J, et al. Assessment of a single-acquisition imaging sequence for oxygen-sensitive (3)He-MRI. Magn Reson Med. 2002;47(1):105–14.
124. van Beek EJ, Dahmen AM, Stavngaard T, Gast KK, Heussel CP, Krummenauer F, et al. Hyperpolarised 3He MRI versus HRCT in COPD and normal volunteers: PHIL trial. Eur Respir J. 2009;34(6):1311–21. doi:10.1183/09031936.00138508.

125. Kirby M, Svenningsen S, Owrangi A, Wheatley A, Farag A, Ouriadov A, et al. Hyperpolarized 3He and 129Xe MR imaging in healthy volunteers and patients with chronic obstructive pulmonary disease. Radiology. 2012;265(2):600–10. doi:10.1148/radiol.12120485.
126. Swift AJ, Wild JM, Fichele S, Woodhouse N, Fleming S, Waterhouse J, et al. Emphysematous changes and normal variation in smokers and COPD patients using diffusion 3He MRI. Eur J Radiol. 2005;54(3):352–8. doi:10.1016/j.ejrad.2004.08.002.
127. Salerno M, de Lange EE, Altes TA, Truwit JD, Brookeman JR, Mugler JP III. Emphysema: hyperpolarized helium 3 diffusion MR imaging of the lungs compared with spirometric indexes—initial experience. Radiology. 2002;222(1):252–60. doi:10.1148/radiol.2221001834.
128. Hermosillo G, Chefd'Hotel C, Faugeras O. Variational methods for multimodal image matching. Int J Comput Vision. 2002;50(3):329–43. doi:10.1023/A:1020830525823.
129. Bauman G, Puderbach M, Deimling M, Jellus V, Chefd'hotel C, Dinkel J, et al. Non-contrast-enhanced perfusion and ventilation assessment of the human lung by means of fourier decomposition in proton MRI. Magn Reson Med. 2009;62(3):656–64. doi:10.1002/mrm.22031.
130. Suga K, Ogasawara N, Okada M, Tsukuda T, Matsunaga N, Miyazaki M. Lung perfusion impairments in pulmonary embolic and airway obstruction with noncontrast MR imaging. J Appl Physiol. 2002;92(6):2439–51. doi:10.1152/japplphysiol.00900.2001.
131. Bauman G, Lutzen U, Ullrich M, Gaass T, Dinkel J, Elke G, et al. Pulmonary functional imaging: qualitative comparison of Fourier decomposition MR imaging with SPECT/CT in porcine lung. Radiology. 2011;260(2):551–9. doi:10.1148/radiol.11102313.
132. Gierada DS, Curtin JJ, Erickson SJ, Prost RW, Strandt JA, Goodman LR. Diaphragmatic motion: fast gradient-recalled-echo MR imaging in healthy subjects. Radiology. 1995;194(3):879–84. doi:10.1148/radiology.194.3.7862995.
133. Suga K, Tsukuda T, Awaya H, Takano K, Koike S, Matsunaga N, et al. Impaired respiratory mechanics in pulmonary emphysema: evaluation with dynamic breathing MRI. J Magn Reson Imaging. 1999;10(4):510–20.
134. Iwasawa T, Takahashi H, Ogura T, Asakura A, Gotoh T, Shibata H, et al. Influence of the distribution of emphysema on diaphragmatic motion in patients with chronic obstructive pulmonary disease. Jpn J Radiol. 2011;29(4):256–64. doi:10.1007/s11604-010-0552-8.
135. Iwasawa T, Yoshiike Y, Saito K, Kagei S, Gotoh T, Matsubara S. Paradoxical motion of the hemidiaphragm in patients with emphysema. J Thorac Imaging. 2000;15(3):191–5.
136. Millner MR, McDavid WD, Waggener RG, Dennis MJ, Payne WH, Sank VJ. Extraction of information from CT scans at different energies. Med Phys. 1979;6(1):70–1.
137. Rutherford RA, Pullan BR, Isherwood I. X-ray energies for effective atomic number determination. Neuroradiology. 1976;11(1):23–8.
138. Barbera JA, Riverola A, Roca J, Ramirez J, Wagner PD, Ros D, et al. Pulmonary vascular abnormalities and ventilation-perfusion relationships in mild chronic obstructive pulmonary disease. Am J Respir Crit Care Med. 1994;149(2 Pt 1):423–9. doi:10.1164/ajrccm.149.2.8306040.
139. Hale KA, Niewoehner DE, Cosio MG. Morphologic changes in the muscular pulmonary arteries: relationship to cigarette smoking, airway disease, and emphysema. Am Rev Respir Dis. 1980;122(2):273–8.
140. Peinado VI, Barbera JA, Ramirez J, Gomez FP, Roca J, Jover L, et al. Endothelial dysfunction in pulmonary arteries of patients with mild COPD. Am J Phys. 1998;274(6 Pt 1):L908–13.
141. Barbera JA, Roca J, Ferrer A, Felez MA, Diaz O, Roger N, et al. Mechanisms of worsening gas exchange during acute exacerbations of chronic obstructive pulmonary disease. Eur Respir J. 1997;10(6):1285–91.
142. Sandek K, Bratel T, Hellstrom G, Lagerstrand L. Ventilation-perfusion inequality and carbon dioxide sensitivity in hypoxaemic chronic obstructive pulmonary disease (COPD) and effects of 6 months of long-term oxygen treatment (LTOT). Clin Physiol. 2001;21(5):584–93.
143. Fuld MK, Halaweish AF, Haynes SE, Divekar AA, Guo J, Hoffman EA. Pulmonary perfused blood volume with dual-energy CT as surrogate for pulmonary perfusion assessed with dynamic multidetector CT. Radiology. 2013;267(3):747–56. doi:10.1148/radiol.12112789.
144. Barbera JA, Peinado VI, Santos S. Pulmonary hypertension in chronic obstructive pulmonary disease. Eur Respir J. 2003;21(5):892–905.
145. Ley S, Puderbach M, Fink C, Eichinger M, Plathow C, Teiner S, et al. Assessment of hemodynamic changes in the systemic and pulmonary arterial circulation in patients with cystic fibrosis using phase-contrast MRI. Eur Radiol. 2005;15(8):1575–80. doi:10.1007/s00330-005-2721-1.
146. Alford SK, van Beek EJ, McLennan G, Hoffman EA. Heterogeneity of pulmonary perfusion as a mechanistic image-based phenotype in emphysema susceptible smokers. Proc Natl Acad Sci U S A. 2010;107(16):7485–90. doi:10.1073/pnas.0913880107.
147. Pansini V, Remy-Jardin M, Faivre JB, Schmidt B, Dejardin-Bothelo A, Perez T, et al. Assessment of lobar perfusion in smokers according to the presence and severity of emphysema: preliminary experience with dual-energy CT angiography. Eur Radiol. 2009;19(12):2834–43. doi:10.1007/s00330-009-1475-6.

148. Lee CW, Seo JB, Lee Y, Chae EJ, Kim N, Lee HJ, et al. A pilot trial on pulmonary emphysema quantification and perfusion mapping in a single-step using contrast-enhanced dual-energy computed tomography. Investig Radiol. 2012;47(1):92–7. doi:10.1097/RLI.0b013e318228359a.
149. Chandra D, Lipson DA, Hoffman EA, Hansen-Flaschen J, Sciurba FC, Decamp MM, et al. Perfusion scintigraphy and patient selection for lung volume reduction surgery. Am J Respir Crit Care Med. 2010;182(7):937–46. doi:10.1164/rccm.201001-0043OC.
150. Park TS, Hong Y, Lee JS, Lee SM, Seo JB, Oh YM, et al. Efficacy of bronchoscopic lung volume reduction by endobronchial valves in patients with heterogeneous emphysema: report on the first Asian cases. J Korean Med Sci. 2014;29(10):1404–10. doi:10.3346/jkms.2014.29.10.1404.
151. Gur D, Drayer BP, Borovetz HS, Griffith BP, Hardesty RL, Wolfson SK. Dynamic computed tomography of the lung: regional ventilation measurements. J Comput Assist Tomogr. 1979;3(6):749–53.
152. Herbert DL, Gur D, Shabason L, Good WF, Rinaldo JE, Snyder JV, et al. Mapping of human local pulmonary ventilation by xenon enhanced computed tomography. J Comput Assist Tomogr. 1982;6(6):1088–93.
153. Chae EJ, Seo JB, Goo HW, Kim N, Song KS, Lee SD, et al. Xenon ventilation CT with a dual-energy technique of dual-source CT: initial experience. Radiology. 2008;248(2):615–24. doi:10.1148/radiol.2482071482.
154. Park EA, Goo JM, Park SJ, Lee HJ, Lee CH, Park CM, et al. Chronic obstructive pulmonary disease: quantitative and visual ventilation pattern analysis at xenon ventilation CT performed by using a dual-energy technique. Radiology. 2010;256(3):985–97. doi:10.1148/radiol.10091502.
155. Chae EJ, Seo JB, Lee J, Kim N, Goo HW, Lee HJ, et al. Xenon ventilation imaging using dual-energy computed tomography in asthmatics: initial experience. Investig Radiol. 2010;45(6):354–61. doi:10.1097/RLI.0b013e3181dfdae0.
156. Goo HW, Yu J. Redistributed regional ventilation after the administration of a bronchodilator demonstrated on xenon-inhaled dual-energy CT in a patient with asthma. Korean J Radiol. 2011;12(3):386–9. doi:10.3348/kjr.2011.12.3.386.
157. Kim WW, Lee CH, Goo JM, Park SJ, Kim JH, Park EA, et al. Xenon-enhanced dual-energy CT of patients with asthma: dynamic ventilation changes after methacholine and salbutamol inhalation. AJR Am J Roentgenol. 2012;199(5):975–81. doi:10.2214/AJR.11.7624.
158. Park SJ, Lee CH, Goo JM, Kim JH, Park EA, Jung JW, et al. Quantitative analysis of dynamic airway changes after methacholine and salbutamol inhalation on xenon-enhanced chest CT. Eur Radiol. 2012;22(11):2441–50. doi:10.1007/s00330-012-2516-0.
159. Hachulla AL, Pontana F, Wemeau-Stervinou L, Khung S, Faivre JB, Wallaert B, et al. Krypton ventilation imaging using dual-energy CT in chronic obstructive pulmonary disease patients: initial experience. Radiology. 2012;263(1):253–9. doi:10.1148/radiol.12111211.
160. Honda N, Osada H, Watanabe W, Nakayama M, Nishimura K, Krauss B, et al. Imaging of ventilation with dual-energy CT during breath hold after single vital-capacity inspiration of stable xenon. Radiology. 2012;262(1):262–8. doi:10.1148/radiol.11110569.
161. Thieme SF, Hoegl S, Nikolaou K, Fisahn J, Irlbeck M, Maxien D, et al. Pulmonary ventilation and perfusion imaging with dual-energy CT. Eur Radiol. 2010;20(12):2882–9. doi:10.1007/s00330-010-1866-8.
162. Zhang LJ, Zhou CS, Schoepf UJ, Sheng HX, Wu SY, Krazinski AW, et al. Dual-energy CT lung ventilation/perfusion imaging for diagnosing pulmonary embolism. Eur Radiol. 2013;23(10):2666–75. doi:10.1007/s00330-013-2907-x.
163. Noma S, Moskowitz GW, Herman PG, Khan A, Rojas KA. Pulmonary scintigraphy in elastase-induced emphysema in pigs. Correlation with high-resolution computed tomography and histology. Investig Radiol. 1992;27(6):429–35.
164. Suga K, Kawakami Y, Iwanaga H, Hayashi N, Seto A, Matsunaga N. Assessment of anatomic relation between pulmonary perfusion and morphology in pulmonary emphysema with breath-hold SPECT-CT fusion images. Ann Nucl Med. 2008;22(5):339–47. doi:10.1007/s12149-007-0137-5.
165. Argula RG, Strange C, Ramakrishnan V, Goldin J. Baseline regional perfusion impacts exercise response to endobronchial valve therapy in advanced pulmonary emphysema. Chest. 2013;144(5):1578–86. doi:10.1378/chest.12-2826.
166. Stavngaard T, Sogaard LV, Mortensen J, Hanson LG, Schmiedeskamp J, Berthelsen AK, et al. Hyperpolarized 3He MRI and 81mKr SPECT in chronic obstructive pulmonary disease. Eur J Nucl Med Mol Imaging. 2005;32(4):448–57. doi:10.1007/s00259-004-1691-x.
167. Suga K, Nishigauchi K, Kume N, Koike S, Takano K, Tokuda O, et al. Dynamic pulmonary SPECT of xenon-133 gas washout. J Nucl Med. 1996;37(5):807–14.
168. Amis TC, Crawford AB, Davison A, Engel LA. Distribution of inhaled 99mtechnetium labelled ultrafine carbon particle aerosol (Technegas) in human lungs. Eur Respir J. 1990;3(6):679–85.
169. Crawford AB, Davison A, Amis TC, Engel LA. Intrapulmonary distribution of 99mtechnetium labelled ultrafine carbon aerosol (Technegas) in severe airflow obstruction. Eur Respir J. 1990;3(6):686–92.
170. Cukic V, Begic A. Potential role of lung ventilation scintigraphy in the assessment of COPD. Acta Inform Med. 2014;22(3):170–3. doi:10.5455/aim.2014.22.170-173.

171. Xu J, Moonen M, Johansson A, Gustafsson A, Bake B. Quantitative analysis of inhomogeneity in ventilation SPET. Eur J Nucl Med. 2001;28(12):1795–800. doi:10.1007/s002590100649.
172. Jogi J, Ekberg M, Jonson B, Bozovic G, Bajc M. Ventilation/perfusion SPECT in chronic obstructive pulmonary disease: an evaluation by reference to symptoms, spirometric lung function and emphysema, as assessed with HRCT. Eur J Nucl Med Mol Imaging. 2011;38(7):1344–52. doi:10.1007/s00259-011-1757-5.
173. Suga K, Kawakami Y, Koike H, Iwanaga H, Tokuda O, Okada M, et al. Lung ventilation-perfusion imbalance in pulmonary emphysema: assessment with automated V/Q quotient SPECT. Ann Nucl Med. 2010;24(4):269–77. doi:10.1007/s12149-010-0369-7.
174. Vidal Melo MF, Winkler T, Harris RS, Musch G, Greene RE, Venegas JG. Spatial heterogeneity of lung perfusion assessed with (13)N PET as a vascular biomarker in chronic obstructive pulmonary disease. J Nucl Med. 2010;51(1):57–65. doi:10.2967/jnumed.109.065185.
175. Gan WQ, Man SF, Senthilselvan A, Sin DD. Association between chronic obstructive pulmonary disease and systemic inflammation: a systematic review and a meta-analysis. Thorax. 2004;59(7):574–80.
176. Karadag F, Karul AB, Cildag O, Yilmaz M, Ozcan H. Biomarkers of systemic inflammation in stable and exacerbation phases of COPD. Lung. 2008;186(6):403–9. doi:10.1007/s00408-008-9106-6.
177. Sinden NJ, Stockley RA. Systemic inflammation and comorbidity in COPD: a result of 'overspill' of inflammatory mediators from the lungs? Review of the evidence. Thorax. 2010;65(10):930–6. doi:10.1136/thx.2009.130260.
178. Jones HA, Marino PS, Shakur BH, Morrell NW. In vivo assessment of lung inflammatory cell activity in patients with COPD and asthma. Eur Respir J. 2003;21(4):567–73.
179. Subramanian DR, Jenkins L, Edgar R, Quraishi N, Stockley RA, Parr DG. Assessment of pulmonary neutrophilic inflammation in emphysema by quantitative positron emission tomography. Am J Respir Crit Care Med. 2012;186(11):1125–32. doi:10.1164/rccm.201201-0051OC.
180. Coulson JM, Rudd JH, Duckers JM, Rees JI, Shale DJ, Bolton CE, et al. Excessive aortic inflammation in chronic obstructive pulmonary disease: an 18F-FDG PET pilot study. J Nucl Med. 2010;51(9):1357–60. doi:10.2967/jnumed.110.075903.
181. Coxson HO, Quiney B, Sin DD, Xing L, McWilliams AM, Mayo JR, et al. Airway wall thickness assessed using computed tomography and optical coherence tomography. Am J Respir Crit Care Med. 2008;177(11):1201–6. doi:10.1164/rccm.200712-1776OC.